A method for membrane characterization employing reliable Forward Osmosis experimental data

Sofia Reyes Lombardo

Submitted to the Faculty of Engineering

in partial fulfillment of the requirements for the degree of

Master of Applied Science in Chemical Engineering

Department of Chemical and Biological Engineering

Faculty of Engineering

University of Ottawa

Abstract

Forward osmosis (FO) is an osmotically driven process that uses a high concentration draw solution to pull water across a semipermeable membrane from a feed solution. Wastewater, seawater, or other contaminated water sources may be used as a feed solution. In FO, the final product is not clean water but a diluted draw solution. However, FO may be combined with another process, e.g. reverse osmosis (RO). The resulting hybrid process offers advantages compared to the RO process in, for example, seawater desalination. Thin-film composite (TFC) membranes have been used in pressurized processes such as RO due to their thick porous support layer and their ability to endure high hydrostatic pressures. However, the presence of a thick porous layer is detrimental for FO processes. It is responsible for the internal concentration polarization (ICP) inside the membrane, reducing the osmotic driving force and the overall water flux. The characterization of membranes in FO applications is key for understanding how different intrinsic parameters affect membrane performance. In this work, a previously developed methodology for characterizing TFC membranes was improved. Experimental data was obtained from a laboratory-scale FO system, and the experimental data was used to determine three intrinsic transport parameters, namely the water permeance, the salt permeance and the porous layer structural parameter. With this method, the characterization of TFC membranes can be achieved based exclusively on FO data. A sensitivity analysis has highlighted the impact of the intrinsic transport parameters on an FO membrane performance.

Résumé

L'osmose directe (OD) est un phénomène régit par le principe de l'osmose qui utilise une solution de prélèvement à haute concentration pour aspirer de l'eau à travers une membrane semi-perméable à partir d'une solution d'alimentation de plus faible concentration. Les eaux usées, l'eau de mer ou d'autres sources d'eau contaminées peuvent être utilisées comme solution d'alimentation. En OD, le produit final ne sera pas de l'eau propre, mais une solution de prélèvement diluée. L'OD peut être utilisée comme prétraitement pour une solution d'alimentation en osmose inverse (OI), où la différence de pression osmotique doit être dépassée pour séparer le soluté de l'eau. Le procédé hybride qui en résulte offre des avantages par rapport au procédé OI, comme par exemple, le dessalement de l'eau de mer. Les membranes composites à couche mince (CCM) ont été utilisées dans des procédés sous pression tels que l'OI en raison de leur important support poreux et elles sont capables de supporter des pressions hydrostatiques élevées. Cependant, cette caractéristique est néfaste pour les procédés d'OD, car le support poreux augmentera l'effet de polarisation de concentration interne (PCI) à l'intérieur de la membrane, réduisant ainsi le flux d'eau global. La caractérisation des membranes dans les applications d'OD est essentielle pour comprendre comment différents paramètres intrinsèques affectent les performances de la membrane. Dans ce travail, une méthode complète de caractérisation des membranes CCM a été développée. Les données expérimentales ont été obtenues à partir d'un système d'OD à l'échelle du laboratoire et les données expérimentales ont été utilisées pour déterminer trois paramètres de transport intrinsèques, à savoir la perméance à l'eau, la perméance au sel et le paramètre structurel de la couche poreuse. Avec cette méthode, la caractérisation des membranes CCM peut être réalisée en utilisant exclusivement des données d'OD. Une analyse de sensibilité a clairement mis en évidence l'impact des paramètres de transport intrinsèques sur les performances d'une membrane d'OD.

Acknowledgements

Foremost, I would like to thank my supervisors, Dr. Boguslaw Kruczek and Dr. Jules Thibault, for their amazing support throughout these years. They were always extremely patient with me and were always available if I had any questions. What I have learned from them in the past years has been the best knowledge I have received in my life.

I want to thank my family and friends for always being there for me, especially my parents, my brother and my husband, who pushed me when I felt a lack of confidence. He constantly reminded me of my potential and my ability to achieve success.

I would also like to thank my lab and office mates for making my time at the University of Ottawa a great place to be, as well as their kind guidance in the lab: Du Bai, Amirsajad Atashgar, Shaima Al-Akwaa, Haoyu Wu, Maryam Zamanian and Farhad Asempour. I also want to thank my roommate Rocio, who supported me through really hard times and continues to do so.

Contributions

Sofia Reyes Lombardo wrote all four chapters. Dr. Boguslaw Kruczek and Dr. Jules Thibault revised and corrected all four chapters.

Chapter 2: Performance of TFC membranes using a dynamic experimental method in a Forward Osmosis system.

Du Bai and Dr. Kruczek previously built the forward osmosis system. Dr. Kruczek developed the experimental hypothesis for this work.

Sofia Reyes Lombardo performed the experimental work, including testing the membrane and processing of the experimental data and the derivation of the models, with the support and guidance of Dr. Kruczek and Dr. Thibault.

Chapter 3: Estimation of the permeability and structural parameters in thin-film composite membranes from forward osmosis experimental data.

The estimation of the intrinsic structural parameters using the model from Tiraferri et al. (2013), Martin et al. (2020) and a model developed in this work was carried out by Sofia Reyes Lombardo with the assistance of Dr. Kruczek and Dr. Thibault. These models also allowed performing a sensitivity analysis.

Table of contents

List of Tables

List of Figures

Chapter 1. Introduction

1.1 Introduction

Water scarcity is one of the most urgent concerns affecting our planet [1]. The growing global population has increased the demand for fresh potable water, and currently, over 1 billion people have limited access to fresh water. The United States and some countries in the Middle East have experienced severe droughts in recent years. Urbanization has impacted groundwater resources, so seawater desalination has emerged as a solution to mitigate this issue partly [2].

Desalination is the process of obtaining water suitable for human consumption by removing salt ions, minerals, and other undesired contaminants from seawater [2]. Membrane desalination seems to be one of the best solutions among the water treatment technologies available nowadays [3]. Hippocrates and Aristoteles first observed desalination in the fourth century BC. Still, it was not until the 20^{th} century when Reid and Breton observed how a cellulose acetate (CA) film could reject sodium chloride from an aqueous solution in the reverse osmosis (RO) process. This was the beginning of what is known now as water desalination by RO membranes [4]. Osmosis and reverse osmosis can only work if the membrane separating the two solutions of different solute concentrations allows selective water transport while totally or partly rejecting the transport of dissolved salts.

Seawater desalination using reverse osmosis (RO) membranes became an industrial process more than 50 years ago when Loeb and Sourirajan fabricated the first integrally skinned asymmetric cellulose acetate membranes. In the RO process, the hydraulic pressure must overcome the osmotic pressure of a feed solution, which is associated with a high-energy requirement [5]. For this reason, research has been focused on exploring new desalination technologies that are more energy-efficient [1].

Osmotic pressure, which must be overcome in the RO process, is evaluated by the modified van't Hoff equation.

$$\pi = i\phi CRT \tag{1-1}$$

where π is the osmotic pressure of the solution, i is the dissociation factor of solutes in the solution, ϕ is a correction factor to account for potential non-ideality, C (mol/L) is the molar concentration of a solute in the solution, T (K) is the absolute temperature, and R is the universal gas constant [6]. If there were more than one solute present in the solution, the osmotic pressure would be calculated as a summation of the right-hand term, one for each solute. An increase in the concentration of the solute leads to an increase in the osmotic pressure of the solution. In the absence of external hydraulic pressure, the osmotic pressure is the main driving force for water flow across a semipermeable membrane, separating two solutions with different solute concentrations.

Forward osmosis (FO), which does not resort to an external hydraulic pressure difference, but strictly on the osmotic pressure for water to migrate across a semipermeable membrane, is a promising membrane separation process due to its low energy consumption and low fouling tendency. FO may be used to treat a broad range of contaminated water and seawater [7]. Forward osmosis may be employed to dilute a saline solution before being processed in a RO desalination system, thus reducing the energy demand of the RO process. It is because water production in the RO process requires overcoming the osmotic pressure. Wastewater is an excellent example of a feed solution that can be used in this application. Indeed, wastewater usually comes with low salinity such that its osmotic pressure is less than that of seawater and brackish water. At the same time, the application of wastewater as a feed in the FO process allows concentrating the solid content in the wastewater [8].

Another example of osmotically driven membrane processes (ODMPs) is pressure-retarded osmosis (PRO), which can be used in power generation applications. In this process, the draw solution is pressurized. However, the applied hydraulic pressure is lower than the osmotic pressure. Consequently, water permeating from a low concentration feed solution pushed the pressurized draw solution, thus generating mechanical energy, which can then be converted into electrical energy [9]. The pumping of both solutions through the membrane module represents the only energy requirement for the process [10].

Thin-Film Composite (TFC) membranes were used to study their performance in FO systems and develop a suitable method to characterize them. Cadotte and Rozelle developed TFC-RO membranes in the early 1970s [11],[12]. This type of membrane is produced by depositing a thin layer of a salt rejecting polyamide (PA) polymer on top of a porous substrate, such as polysulphone (PS), by an interfacial polymerization reaction [4].

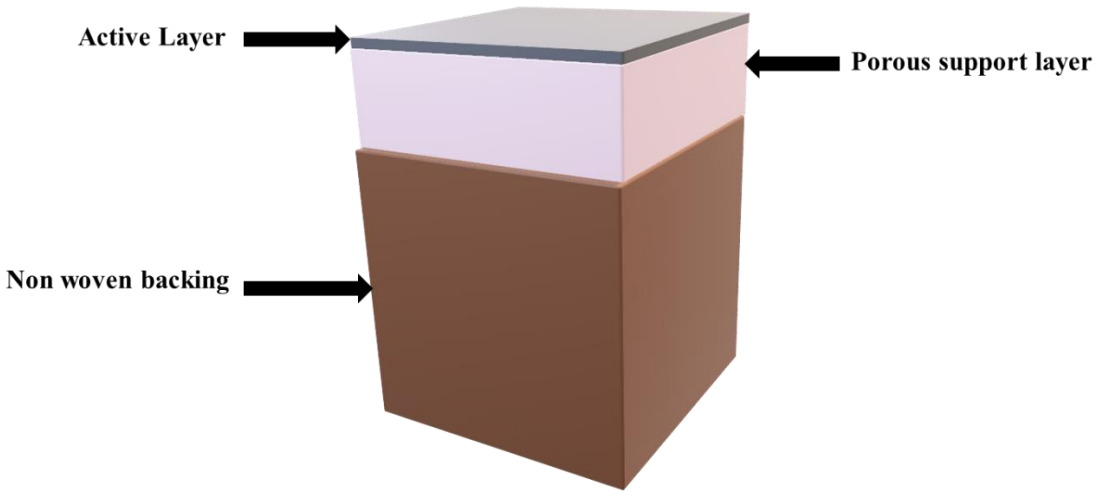

Figure 1.1. Schematic diagram of a TFC membrane showing the thin active layer supported by the porous support layer and a non-woven backing layer [13].

TFC membranes are typically composed of three layers. The first layer is known as the active layer made of polyamide (PA) with a thickness of 500 nm or less. The hydrophilicity of the active layer and pore size allow the water to permeate through this layer while significantly restricting the permeation of salt. This PA layer is formed by interfacial polymerization, where m-phenylenediamine (MPD) reacts with trimesoyl chloride (TMC) [1]. The second layer, made of polysulfone or polyethersulfone, is known as the porous support layer as it serves as the backing to support the active layer. This layer provides a positive physical resistance but creates a detrimental additional mass transfer resistance in FO processes, as it increases the effect of the internal concentration polarization (ICP). Finally, a relatively thicker layer comprised of non-woven backing support is included such that the membrane can endure high pressures during RO processes [14]. This layered fabrication allows using material combinations to achieve optimal

performance and durability of the membrane in pressure-driven processes. Membrane production has mostly been focused on pressure-driven, not osmotically-driven, processes. The porous support layer in TFC membranes provides the necessary physical integrity to sustain high pressures. However, this porous support is detrimental for FO processes, as it will increase the effect of ICP [15].

A semipermeable membrane inevitably induces the phenomenon of concentration polarization (CP) that has a detrimental effect on water flux (J_w). Given the selective transfer of water through the membrane under the effect of transmembrane driving forces, CP refers to the inception of a concentration gradient at the solution/membrane interface. The preferential flow of water through the membrane decreases the interface solute concentration on the draw side. Simultaneously, the interface solute concentration on the feed side increases, reducing the concentration gradient across the active layer of the membrane and hence the osmotic pressure gradient. This CP phenomenon is classified as external concentration polarization (ECP) when it occurs in the fluid boundary layer adjacent to the active layer of the membrane and as internal concentration polarization (ICP) when the CP occurs inside the porous support of the active layer. The effects of ECP can be partly mitigated by physical means, such as increasing the velocity of the solution or adding a mixing device. On the other hand, ICP cannot be reduced by these means. The only solution to minimize the ICP is to develop a membrane specific for FO applications with a thinner support layer of high porosity. Figure 1.2 provides a schematic diagram of solute concentration profiles in a TFC membrane operated in two different orientations; active layer facing draw solution (AL-DS) and active layer facing feed solution (AL-FS). The two membrane orientations are also referred to as PRO (Fig. 1.2a) and FO (Fig. 1.2b) modes, respectively. The term PRO should not be confused with the PRO process (Pressure Retarted Osmosis). PRO mode refers exclusively to the membrane orientation in which the active layer is facing the draw solution. On the other hand, the term FO may refer to either the membrane orientation in which the active layer is facing the feed solution or the process of Forward Osmosis. The two membrane orientations have been studied extensively as it has been shown that each orientation will yield different water and solute fluxes [15-17].

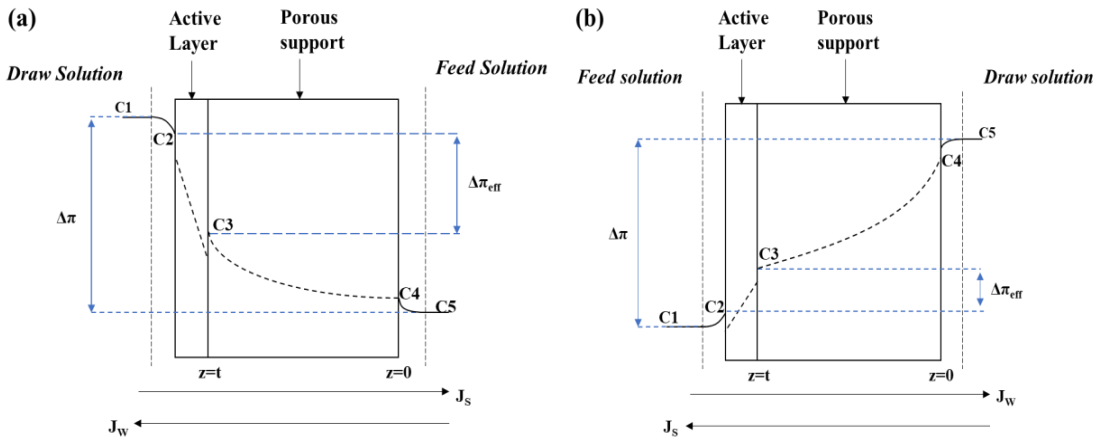

Figure 1.2. Schematic diagram showing the solute concentration profile across the membrane illustrating the ECP and ICP phenomena in a TFC membrane operated in (a) AL-DS mode and (b) AL-FS mode.

1.2 Thesis Objectives

In performing experiments with TFC membranes, the characterization of membranes is mainly impacted by the variability of the membrane per se and the experiment-to-experiment variability. To properly characterize the properties of a TFC membrane under the same or various operating conditions, it is essential to remove the coupon-to coupon variability. This implies that the membrane must be regenerated between two experiments so that the state of the membrane after regeneration is essentially identical to the initial state of the coupon being tested. This thesis hypothesizes that a single membrane coupon can be used and then regenerated between two successive experiments to bring the membrane to its original state to perform a large number of experiments given its characterization. In this work, eighteen experiments, including three replicates for each experimental condition, were carried out using the same membrane coupon. The results were analyzed and used for the membrane characterization. The main objective of this thesis is to develop a proper membrane cleaning protocol to regenerate the membrane between successive experimental tests. Two membrane cleaning methods were tested in this investigation. The membrane coupon was tested in the AL-DS and AL-FS orientations, employing three draw solution concentrations. Each test was repeated three times to ensure the results were reliable. The

results were compared to Bai and Kruczek work [20], who used a different coupon for each experimental test to evaluate the reduction in variability. The experimental results for water and salt fluxes were used to characterize the membranes employing two models from the literature and one developed in this work. The two models from the literature allowed for the calculation of three parameters *A*, *B* and *S* (water permeance, solute permeance and the structural parameter). The model developed in this work allowed for the calculation of *A* and *B*.

1.3 Structure of Thesis

The thesis consists of four chapters. The first chapter presents a general introduction to forward osmosis and the objectives of this research work. Chapters 2 and 3 contain manuscripts to be submitted to peer-reviewed journals based on the two main topics of the thesis. As this is a paper-based thesis and, for the sake of completeness, some concepts may be repeated throughout the thesis. Chapter 4 contains a general conclusion and recommendations for future work. Appendices A and B contain the detailed derivation of the two literature models used in Chapter 3.

NOMENCLATURE

A	Water permeance	L/m^2 h bar
B	Salt permeability	g/m^2 h
C	Molar concentration of a solute in the solution	mol/L
C_1	In the AL-DS orientation, it represents the salt concentration in the bulk draw solution. In the AL-FS, it represents the salt concentration in the bulk feed solution.	mol/L
C_2	In the AL-DS orientation, it represents the salt concentration in the membrane surface at the active layer side towards the draw solution. In the AL-FS orientation, it represents the salt concentration in the membrane surface at the active layer side towards the feed solution.	mol/L
C_3	In the AL-DS and AL-FS orientations, it represents the salt concentration inside the membrane at the interface between the active layer and the porous support.	mol/L
C_4	In the AL-DS orientation, it represents the salt concentration in the membrane surface at the porous support layer side towards the feed solution. In the AL-FS orientation, it represents the salt concentration in the membrane surface at the porous support layer side towards the draw solution.	mol/L
C_5	In the AL-DS orientation, it represents the salt concentration in the bulk feed solution. In the AL-FS orientation, it represents the salt concentration in the bulk draw solution.	mol/L
$\Delta\pi$	Osmotic pressure difference	bar
$\Delta\pi_{eff}$	Effective osmotic pressure gradient	bar
i	Dissociation factor of solutes in the solution	-
J_s	Salt flux	g/m^2 h
J_w	Water flux	L/m^2 h
R	Universal gas constant	bar L/mol K
S	Structural parameter	m
T	Absolute temperature	K

Subscripts

D	Draw solution
F	Feed solution
S	Salt
W	Water

Greek letters

π	Osmotic pressure	bar
Φ	Correction factor	-

Abbreviations

AL-DS	Active Layer facing the Draw Solution
AL-FS	Active Layer facing the Feed Solution
CA	Cellulose Acetate
CP	Concentration Polarization
ECP	External Concentration Polarization
FO	It may refer to Forward Osmosis or to the membrane orientation in which the Active Layer is facing the Feed Solution
ICP	Internal concentration polarization
MPD	M-phenylenediamine
ODMP	Osmotically Driven Membrane Processes
PA	Polyamide
PRO	It refers to Pressure Retarded Osmosis or the membrane orientation in which the Active Layer is facing the Draw Solution
PS	Polysulfone
RO	Reverse Osmosis
TFC	Thin Film Composite Membrane
TMC	Trimesoyl Chloride

References

[1] M. Qasim, N. A. Darwish, S. Sarp, and N. Hilal, "Water desalination by forward (direct) osmosis phenomenon: A comprehensive review," *Desalination*, vol. 374, pp. 47–69, 2015.

[2] F. Nave, R. Kommalapati, and A. Thompson, "Introductory Chapter: Osmotically Driven Membrane Processes," *IntechOpen*. Pages 1-11, 2018. http://dx.doi.org/10.5772/intechopen.72569

[3] H. Zheng, "General Problems in Seawater Desalination," in *Solar Energy Desalination Technology*, Elsevier, 2017, pp. 1–46s https://doi.org/10.1016/B978-0-12-805411-6.00001-4

[4] R. Singh and N. P. Hankins, *Introduction to Membrane Processes for Water Treatment*. Elsevier B.V., 2016. https://doi.org/10.1016/B978-0-444-63312-5.00002-4

[5] J. Kucera, Reverse Osmosis: Industrial Processes and Applications, Second Edition, Second, John Wiley & Sons, Inc., 2015. doi:10.1002/9781119145776.ch4.

[6] J.C. Crittenden, R.R. Trussell, D.W. Hand, K.J. Howe, G. Tchobanoglous, Reverse Osmosis, in: MWHs Water Treat. Princ. Des. Third Ed., John Wiley & Sons, Inc., 2012: pp. 1335– 1414

[7] P. Xiao *et al.*, "A sacrificial-layer approach to fabricate polysulfone support for forward osmosis thin-film composite membranes with reduced internal concentration polarisation," *J. Memb. Sci.*, vol. 481, pp. 106–114, 2015.c https://doi.org/10.1016/j.memsci.2015.01.036

[8] T. Y. Cath, N. T. Hancock, C. D. Lundin, C. Hoppe-Jones, and J. E. Drewes, "A multi-barrier osmotic dilution process for simultaneous desalination and purification of impaired water," *J. Memb. Sci.*, vol. 362, no. 1–2, pp. 417–426, 2010. https://doi.org/10.1016/j.memsci.2010.06.056

[9] T. Y. Cath, M. Elimelech, J. R. McCutcheon, R. L. McGinnis, A. Achilli, D. Anastasio, A. R. Brady, A. E. Childress, I. V. Farr, N. T. Hancock, J. Lampi, L. D. Nghiem, M. Xie, N. Y. Yip, "Standard Methodology for Evaluating Membrane Performance in Osmotically Driven Membrane Processes," *Desalination*, vol. 312, pp. 31–38, 2013. https://doi.org/10.1016/j.desal.2012.07.005

[10] A. Haupt and A. Lerch, “Forward osmosis application in manufacturing industries: A short review,” *Membranes (Basel).*, vol. 8, no. 3, 2018. https://doi.org/10.3390/membranes8030047

[11] J. E. Cadotte, R. J. Petersen, R. E. Larson, and E. E. Erickson, “A new thin-film composite seawater reverse osmosis membrane,” *Desalination*, vol. 32, no. C, pp. 25–31, 1980.

[12] W. J. Lau, A. F. Ismail, N. Misdan, and M. A. Kassim, “A recent progress in thin-film composite membrane: A review,” *Desalination*, vol. 287, pp. 190–199, 2012.

[13] J. A. Idarraga-Mora, A. S. Childress, P. S. Friedel, D. A. Ladner, A. M. Rao, and S. M. Husson, “Role of nanocomposite support stiffness on TFC membrane water permeance,” *Membranes (Basel).*, vol. 8, no. 4, pp. 3–5, 2018. https://doi.org/10.3390/membranes8040111

[14] A. Shrivastava,, & D. Stevens, "Energy Efficiency of Reverse Osmosis". In Sustainable Desalination Handbook: Plant Selection, Design and Implementation. 2018 https://doi.org/10.1016/B978-0-12-809240-8.00002-2

[15] J. R. McCutcheon and M. Elimelech, “Influence of concentrative and dilutive internal concentration polarization on flux behavior in forward osmosis,” *J. Memb. Sci.*, vol. 284, no. 1–2, pp. 237–247, 2006. https://doi.org/10.1016/j.memsci.2006.07.049

[16] D. H. Jung, J. Lee, D. Y. Kim, Y. G. Lee, M. Park, S. Lee, D. R. Yang, J. H. Kim, “Simulation of forward osmosis membrane process: Effect of membrane orientation and flow direction of feed and draw solutions,” Desalination, vol. 277, no. 1–3, pp. 83–91, 2011.

[17] C. Y. Tang, Q. She, W. C. L. Lay, R. Wang, and A. G. Fane, “Coupled effects of internal concentration polarization and fouling on flux behavior of forward osmosis membranes during humic acid filtration,” J. Memb. Sci., vol. 354, no. 1–2, pp. 123–133, 2010.

[18] A. Tiraferri, N. Y. Yip, A. P. Straub, S. Romero-Vargas Castrillon, and M. Elimelech, “A method for the simultaneous determination of transport and structural parameters of forward osmosis membranes,” *J. Memb. Sci.*, vol. 444, pp. 523–538, 2013. https://doi.org/10.1016/j.memsci.2013.05.023

[19] J. T. Martin, G. Kolliopoulos, and V. G. Papangelakis, “An improved model for membrane characterization in forward osmosis,” *J. Memb. Sci.*, vol. 598, no. November 2019, p. 117668, 2020. https://doi.org/10.1016/j.memsci.2019.117668

[20] D. Bai, B. Kruczek, Effect of membrane orientation and concertation of draw solution on behaviors of commercial low-pressure RO membrane in novel dynamic forward osmosis tests, under review in Desalination

Chapter 2

Improving the accuracy of dynamic Forward Osmosis experiments

Sofia Reyes-Lombardo, Jules Thibault, Boguslaw Kruczek*

Department of Chemical & Biological Engineering
University of Ottawa
161 Louis Pasteur Street
Ottawa, ON K1N 6N5, Canada

*** To whom correspondence should be addressed.**

Chapter 2. Improving the accuracy of dynamic Forward Osmosis experiments

Abstract

Membrane performance is key to understanding the opportunities and limitations of osmotically driven membrane processes (ODMP). Forward osmosis (FO) is a promising ODMP that employs the osmotic pressure difference between a feed and a draw solution prompting the mass transport of water across a semipermeable membrane from the feed to the draw side. Thin-film composite (TFC) membranes have been widely used in reverse osmosis (RO) due to their high-water flux and salt rejection. However, a multilayer porous support of TFC membranes, necessary to provide mechanical integrity of the membrane in the RO process, is responsible for the interfacial concentration polarization in FO processes, reducing the overall water flux. There is no optimal FO commercial membrane that yields high water flux and low reverse solute flux. Developing FO membranes with optimized transport properties requires a reliable membrane characterization method. In this work, we developed in-situ membrane cleaning methods to use the same membrane in the entire series of experiments. TFC membranes were tested in a dynamic FO system using three NaCl solution concentrations as draw solution and deionized water as the feed solution, along with two membrane orientations (AL-DS, AL-FS). Each test was repeated three times at identical experimental conditions to validate that using the same membrane coupon could reduce the variation between results compared to when a new membrane coupon is inserted in each test. These results were compared to Bai et al. (2020) work, in which eighteen different membrane coupons were tested using the FO dynamic system presented next. Current results demonstrate that in-situ membrane cleaning partly reduces variation in the experimental results and generally yields the expected qualitative trends.

2.1 Introduction

Water scarcity is considered a global emergency [1]. Due to the increase in population, the demand for fresh potable water has increased, and currently, over 1 billion people have limited access to freshwater. Urbanization has also impacted groundwater resources [2]. The most challenging step in producing drinkable water from brackish and seawater is removing monovalent ions, which is referred to as desalination [3]. Reverse osmosis (RO) membrane separation is the dominating desalination technology. In this process, a semipermeable membrane is used to reject salt while allowing pure water to permeate across the membrane under a hydraulic pressure gradient, which exceeds the osmotic pressure gradient. Overcoming the osmotic pressure, which is very high, particularly in seawater desalination, results in a high energy requirement [4].

In the absence of a hydraulic pressure gradient, water is transported from a low concentration side into a high concentration side across a semipermeable membrane [5], and the process is referred to as osmosis (known for centuries) or, more recently as forward osmosis (FO) [6]. Unlike RO, FO does not produce pure water. However, FO can be combined with RO to decrease the energy requirement in water production by desalination. In this case, FO is used as a pretreatment step in which high salinity feed (e.g. seawater) is diluted, which reduces the required hydraulic pressure in the subsequent RO process. The water for diluting seawater can be drawn from any low-salinity source, for example, wastewater. Thus "impaired water" is suitable for this hybrid FO-RO process [7]. FO can also draw fresh water directly from seawater employing a synthetic draw solution, which generates osmotic pressure higher than seawater. Therefore, the synthetic draw solution is diluted in the FO process and has to be reconcentrated in a subsequent process (typically RO), in which the pure water is produced. The advantage of this hybrid FO-RO process is the possibility of skipping some pretreatment steps. Since FO does not require applied hydraulic pressure, membrane fouling, one of the biggest challenges of RO desalination, is significantly reduced [8],[9]. Further examples of FO applications include emergency water supply with so-called hydration bags [10], treatment of wastewater from oil and gas production and mining [11], biological wastewater treatment with osmotic membrane bioreactors [12], treatment of anaerobic digester concentrate [13], and others [14].

RO membrane desalination is a mature technology, and any RO membrane can be used in a FO process. Thin-film composite (TFC) membranes dominate the RO market. TFC membranes consist of three layers, a selective polyamide layer formed by interfacial polymerization on a support layer - typically ultrafiltration (UF) membrane – and nonwoven support. The role of the UF and nonwoven layers is to provide mechanical support for the selective layer for membranes. RO processes require hydraulic feed pressures above 50 atm. However, when a TFC membrane is used in an FO process, the UF and nonwoven layers cause internal concentration polarization (ICP), which dramatically reduces the productivity (water flux) of the FO process. Unlike RO, only a few commercial membranes designed explicitly for FO applications are available on the market, and membrane development is currently the focus of FO research. An ideal FO membrane should consist of a selective (similar to the RO membrane) on a support layer, not imposing an excessive ICP. In other words, the support should be thin and porous, as the FO process (unlike the RO process) does not require any applied hydraulic pressure.

2.2 Theoretical background

Forward osmosis membranes are characterized by three parameters, namely the water permeance (A), the salt permeance (B) and the structural parameter (S), using a so-called RO-FO method. The A and B are evaluated from the experimentally measured water flux (J_w) and salt flux (J_s) determined in RO experiments, where:

$$J_w = A(\Delta p - \Delta \pi) \tag{2-1}$$

$$J_S = B\Delta c \tag{2-2}$$

where: Δp and $\Delta \pi$ are the hydraulic and osmotic pressure gradients across the membrane, respectively, and Δc is the solute concentration gradient In turn, $\Delta \pi$ and Δc are correlated via the van't Hoff equation:

$$\Delta \pi = \Delta ciRT \tag{2-3}$$

where: i is the number of ionic species each molecule will dissociate, and c is the molar concentration of solute. Knowing A and B, the structural parameter S is calculated from J_w and J_s

measured in FO tests. The structural parameter determines the ICP and depends on the morphology of the porous sublayer of FO membrane:

$$S = \frac{t\tau}{\varepsilon_{eff}} \tag{2-4}$$

where: t, τ, and ε_{eff} are the thickness, tortuosity and effective porosity of the support layer.

Eqs. (2-1) and (2-2) cannot be used directly because the concentration at the interface between the active and support layer is unknown due to ICP. In addition, when the ECP is not negligible, the concentration at the interface between the active layer and the surrounding solution is also unknown. Thus, specific equations that embed these additional mass transfer resistance must be used to estimate the permeance parameters *A* and *B*. These equations are presented and used in Chapter 3 to estimate the intrinsic membrane parameters *A*, *B* and *S*.

The standard RO-FO characterization method was criticized because of the reliance on RO tests. RO tests require Δp, which may lead to membrane compaction. As a result, *A* and *B* might be affected by the applied pressure. In other words, *A* and *B* determined in RO tests might be different from *A* and *B* that prevail in FO tests in the absence of Δp. Since *S* depends on *A* and *B*, it might not represent the same FO membranes not exposed to Δp. Moreover, in the RO test, solute and water move in the same direction, whereas in the FO test, they move in the opposite direction. Consequently, alternative ways to characterize FO membranes were proposed, which rely solely on a series of FO tests. Tiraferri et al. [15] proposed a method for the simultaneous determination of transport and structural parameters of FO membrane in a multi-stage FO experiment. In each subsequent stage, the concentration of the draw solution gradually increases, and steady-state J_w and J_s are recorded. The values of *A*, *B* and *S*, are determined by modelling the transport of solute and water in the TFC FO membrane. This method, which does not rely on RO tests, was further modified by others [16],[17]. However, both the previous RO-FO and the newer only-FO methods rely solely on steady-state tests.

The FO membrane can be operated with the active (selective) layer facing a draw solution (AL-DS) or with the active (selective) layer facing a feed solution (AL-FS). Fig. 2.1 presents the concentration profile of solute schematically in FO membrane operated in AL-DS (Fig. 2.1a) and

AL-FS (Fig. 2.1b) orientations. In the absence of Δp, the water flux, given by Eq. (2-1) simplifies to:

$$J_w = -A\Delta\pi_{eff} \tag{2-5}$$

The negative sign signifies that water transport takes place in the direction of the increasing solute concentration, which is the opposite direction to the transport of the solute. $\Delta\pi_{eff}$ is based on the active layer's concentration gradient ($c_2 - c_3$ or $c_3 - c_2$) rather than the draw and feed side ($c_1 - c_5$ or $c_5 - c_1$). Consequently, $\Delta\pi_{eff}$ is less than $\Delta\pi$, which decreases the water flux (the productivity) in the FO process. The concentration gradient adjacent to the active layer ($c_1 - c_2$) is due to resistance to solute diffusion in the film next to the active layer, referred to as the external concentration polarization (ECP). Some researchers also include ECP at the porous substrate's interface [16],[18]. The effects of the ECP can be minimized (even eliminated) by inducing turbulence at both surfaces of the FO membrane. On the other hand, the concentration gradient within the porous substrate, i.e. internal concentration polarization (ICP) due to resistance to diffusion of solute in the liquid within the porous substrate, is not affected by turbulence at the external surfaces of the membrane. The magnitude of this resistance is directly proportional to the structural parameter of the FO membrane.

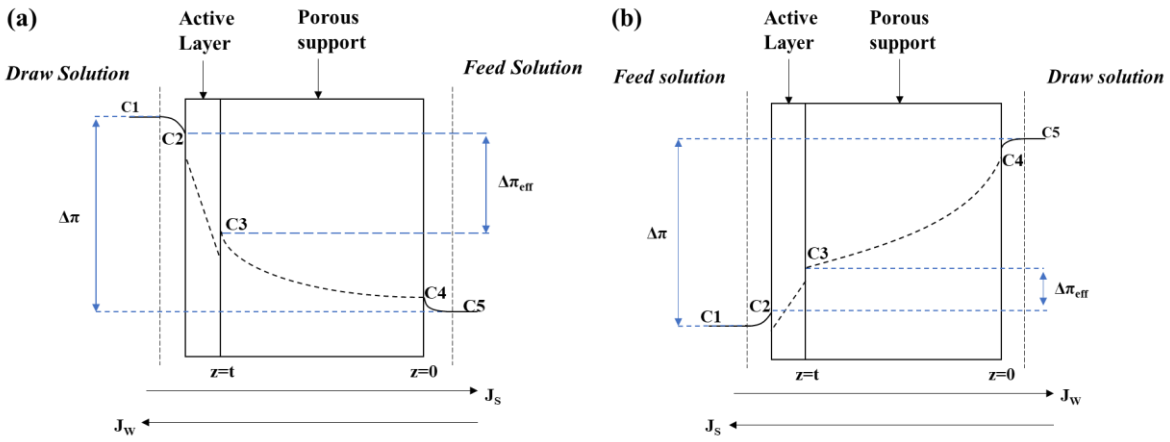

Figure 2.1. Qualitative representation of the concentration profile of the draw solute in a TFC-FO membrane operated in (a) AL-DS orientation (concentrative ICP and dilutive ECP), and (b) AL-FS orientation (dilutive ICP and concentrative ECP).

In gas permeation membranes, the resistance to gas diffusion across the membrane is directly proportional to a time lag, an experimentally measurable parameter. In turn, the measurement of time lag requires the execution of a dynamic test, in which the membrane, initially in equilibrium or at steady state, is subjected to a step-change in a driving force for the transport of permeating species, and accurate monitoring of the resulting change in the permeation rate. Although the time-lag method is widely used to characterize gas permeation membranes, it is absent in the characterization of liquid permeation membranes, including TFC-FO membranes. It is because of the difficulty in executing a step-change in the driving force for permeation of species, i.e., in a controllable initiation of a dynamic experiment.

We have recently described a protocol that allows a sudden change of a draw solution concentration in a modified FO testing system [19] and accurate monitoring of the progress of the resulting dynamic experiment. More specifically, following the step change, we monitored the masses of the draw and the feed solutions and the conductivity of the feed solution in real-time. We demonstrated the applicability of the new method by performing a series of dynamic FO tests in AL-DS and AL-FS orientations using a commercial low-pressure RO membrane. For each membrane orientation and the draw solution concentration, the tests were performed in triplicates. Each test utilized different coupons cut from the same commercial membrane. We observed a considerable variation in the water and salt time lags for a given condition, which we attributed to the variation of properties from coupon to coupon. The ultimate goal of determining the water and salt time lags in dynamic FO experiments is the experimental determination of the structural parameter of the characterized FO membrane, which requires consistent experimental results. The water and salt time lags were used as a measurement of variability when comparing experimental results. Therefore, in this paper, we explore an alternative approach. Instead of changing a membrane coupon in each experiment, including the repeated tests, we propose using the same coupon in all experiments and thoroughly cleaning it between the tests without removing the coupon from the membrane cell. To assess the suitability of the new approach, we repeated the characterization of the same commercial TFC-FO membrane as in ref. [19] and compared the variability of the experimental results in the original and the modified approaches.

2.3 Materials and methods

2.3.1 Forward osmosis testing system

The heart of the time-lag method is the testing system and experimental protocol that was described previously [19]. The main components of the testing system shown in Fig. 2.2 include a Teflon crossflow symmetric membrane cell (CF016D-FO Cell, Sterlitech, USA) with effective permeation area and hold up volume of 20.6 cm^2 and 4.7 cm^3, two balances B1 (0.1 g resolution, PA4201C, Pioneer, Ohaus, USA) and B2 (0.01 g resolution, 6202-1S, Entris Precision, Sartorius, Germany) for the feed and draw solutions tanks (1-L capacity each), two pumps P1 and P2 (TE-3-MD-HC, Little Giant Co., USA), two 0-4 LPM flowmeters, FM1 and FM2 (Blue-White Industries Ltd., USA), two 100-120 kPa (0-3 psig) pressure gauges PG1, PG2 (McMaster-Carr, USA), two heat exchangers HEX1 and HEX2 connected to an Isotemp R20 Refrigerated and Heated Bath Circulator (Model 4100 R20, Fisher Scientific, USA), and a benchtop conductivity/temperature meter, T-C (CON2700, Oakton Instruments, USA). The T-C meter could be moved between the draw and feed solution tanks. However, it is used in the draw solution tank only before and after the experiment. Immediately before and during the tests, the T-C meter resides in the feed-solution tank. The two parts of the system for the circulation of the feed and draw solutions are practically similar. The only difference is the length of polypropylene tubing (No. 5392K14, OD = 0.95 cm (3/8"), ID = 0.63 cm (1/4"), McMaster-Carr, USA), which are 2.0 m on the draw side and 1.8 m on the feed side. The critical element that allows a sudden change in the draw solution concentration is a bypass. The system included two bypasses BP1 and BP2, one on each side. The length of tubing in each bypass is minimized (30 cm) with the corresponding volumes of 9.5 cm^3. In addition, the system includes four three-way valves V3, V4, V5, V6 (No.4757K62, McMaster-Carr, USA) and regular ball valves V1, V2 (No.4757K22, McMaster-Carr, USA). The three-way valves allow alternating the draw and feed solutions streams between the membrane cell and the respective bypass lines to initiate the dynamic permeation experiment.

The balances and the conductivity meter were connected to a computer that recorded the experimental data every 2.5 seconds, employing a LabView data acquisition program, which allowed monitoring of the progress of the entire tests in real-time.

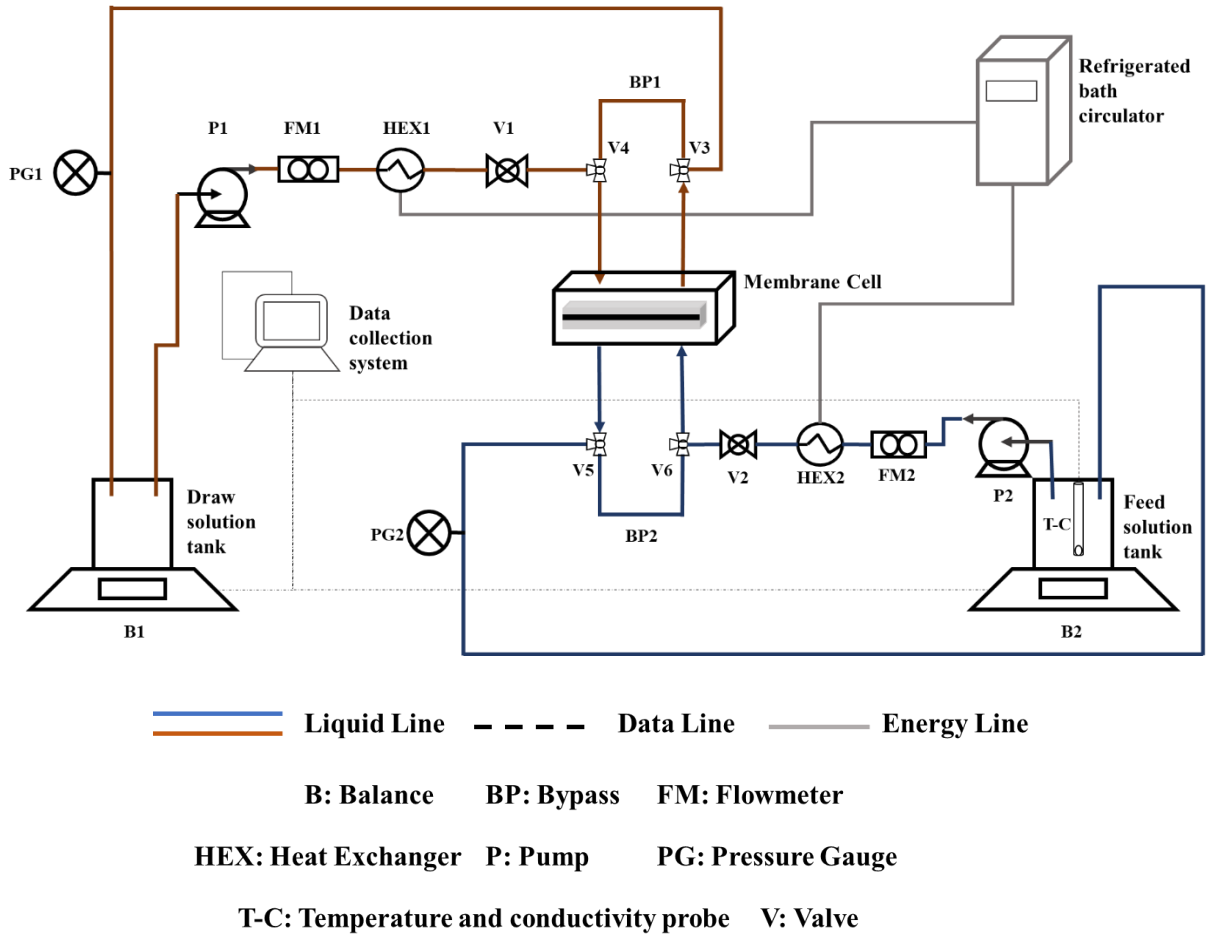

Figure 2.2 Schematic diagram of the Forward Osmosis testing system [19].

The membrane used in this work was a commercial low-pressure RO TFC membrane with test conditions of 500 mg/L aqueous NaCl feed solution at 860 kPa (110 psig) and 25°C, the maximum flow rate of 32.7 L/m^2 h and 99% salt rejection (Toray Industries Inc, 2021), i.e. similar to the one used in our previous work [19]. The membrane comprises three layers: the active (selective) polyamide layer, a polysulfone (PS) support layer, and a nonwoven fibre support layer made of polyethylene terephthalate (PET). Although the morphologies of the PS and PET layers are different, they are both nonselective and correspond to the porous support in Fig. 2.1.

2.3.2 Experimental protocol

A dynamic experiment requires a step-change in a driving force, which for FO tests is a concentration gradient between the draw solution and the feed solution. The system shown in Fig. 2.1 allows a sudden change in the draw solution concentration for zero (distilled water) to any desired value. The main objective of this paper is to generate reliable dynamic data on the effect of the step change and the membrane orientation when characterizing a low-pressure RO TFC membrane. This data was already generated but using different membrane coupons in each dynamic experiment. However, it was suspected that the previously generated data could be influenced by variation in the properties of coupons, thus obscuring the actual effects of the membrane orientation and the draw solution concentration. In the current study, we follow a similar experimental protocol as in ref. [19], except the same membrane is used in all experiments. It requires a thorough cleaning of the membrane between the tests to remove the draw solute – NaCl. We explored two different cleaning approaches, which are described below.

After the installation of a membrane in the cell, both the feed and the draw sides of the membrane and the bypasses BP1 and BP2 were thoroughly cleaned by circulating deionized (DI) water. The cleaning process continued until the conductivity on both sides of the membrane reached the minimum detection level of 30 µs/cm. At this point, the flow on both sides of the membrane was directed through the bypasses BP1 and BP2, while both sides of the membrane remained exposed to DI water. In the next step, the volume of DI water in the feed tank solution was adjusted to 400 mL, while the DI water in the draw solution tank was replaced by 700 mL of the draw solution at the desired concentration. These volumes were tailored to strike a balance between maintaining relatively constant the driving force and detecting the concentration changes in the feed solution. With the feed and draw solution tanks charged with appropriate solutions, the flow rate of both the feed and draw solutions was set at 2.4 L/min (the maximum controllable flow rate available from the TE-3-MD-HC centrifugal pumps) using the appropriate pumps and valves. The feed and draw solutions were circulated through the bypasses BP1 and BP2 until the desired experimental temperature was reached. The temperature on both sides of the membrane was controlled using the respective HEX connected to the refrigerated bath circulator. Once the system reached the steady-state, i.e., the flow rates and temperature were constant, the step change was

initiated by manually redirecting the draw and feed solutions from the bypasses BP1 and BP2 to the draw side and the feed side of the membrane cell, respectively. This process of redirecting the streams was accomplished in less than 2 s.

After completing the first experiment, the membrane and the entire system were cleaned using distilled water. With the coupon in the membrane cell, the content in the draw and feed solution tanks was replaced by the fresh distilled water. Both sides of the system were set to bypass mode, and the pumps were turned on. The water circulation continued until the conductivity in the draw and feed solution tanks reached a constant value. At this point, the bypass lines were closed, and the flow was directed to the membrane cell. The cleaning of the membrane cell continued until the conductivity in the tanks reached a constant value. Then, the liquid in both tanks was replaced by fresh distilled water, and the cleaning procedure was repeated. The water in the draw and feed solution tanks changed 20 times. In the first approach (Membrane 1), in all 20 steps, distilled water was used. In the second approach (Membrane 2), the DI water was used from the 11^{th} step onward. The cleaning continued until the conductivity in both tanks dropped below 90 μs/cm when using the distilled water (1^{st} approach) or 50 μs/cm when using the DI water (2^{nd} approach).

We switched the draw and feed solution tanks to convert from the AL-DS orientation to the AL-FS orientation without removing the coupon from the cell. In total, three different step changes in the draw solution concentrations from 0 to 1, 2, and 4 mol/L and two membrane orientations were considered. Therefore, each membrane was tested at six different experimental conditions, and each test was repeated three times. Consequently, 18 experiments were performed with Membrane 1 (first cleaning approach) and 18 with Membrane 2 (second cleaning approach).

The processing of experimental data from the dynamic experiments was described elsewhere [19]. Despite covering the draw and feed containers with a paraffin film, we observed some water evaporation. Since the feed and draw solutions in Fig. 2.1 circulate in closed loops, the total mass of water, at any time, should be constant regardless of the water transport across the membrane. However, we observed a slight decrease in the total mass of water, which increased linearly with time. To correct for the evaporation of water, we used a correction factor (a) such that:

$$m_{D,\mathrm{cor}} = m_D - at \tag{2-6}$$

$$m_{F,\mathrm{cor}} = m_F + at \tag{2-7}$$

$$m_{T,\mathrm{cor}} = m_{D,\mathrm{cor}} + m_{F,\mathrm{cor}} = 0 \tag{2-8}$$

where, m is the mass at time t, the subscripts D, F, and T refer to draw, feed and the total masses, while subscript *cor* refers to the corrected value. In addition, switching the system from the bypass to membrane configuration at the initiation of the dynamic experiment led to a step-change in the mass of the feed and draw solutions, which was not related to the water transport across the membrane [19]. The initial masses of the feed and draw solutions were adjusted accordingly, such that $m_D(0) = m_F(0) = 0$. Since the data was recorded every 2.5 s, there was some ambiguity when zeroing m_D and m_F.

The mass of draw solute (NaCl) in the feed solution at time t (m_{NaCl}) was calculated:

$$m_{\mathrm{NaCl}} = m_F \cdot c_{\mathrm{NaCl}} \tag{2-9}$$

where: c_{NaCl} [mg/L] was determined for the conductivity of the feed solution measured using the T-C meter. The calibration of the T-C meter using fixed concentrations of NaCl was performed regularly between the dynamic experiments. It is important to note that Eq. (2-9) does not require the corrected mass of the feed solution. Regardless of the cleaning procedure, i.e. the initial conductivity of the feed solution (< 90 μS/cm or < 50 μS/cm), the initial mass of NaCl in the feed solution was assumed to be zero.

Eqs. (2-6)-(2-9) allow plotting $m_{D,\mathrm{cor}}$, $m_{F,\mathrm{cor}}$ and m_{NaCl} as a function of time. The slope of the linear portions of $m_{D,\mathrm{cor}}$ vs t (or $m_{F,\mathrm{cor}}$ vs t) and m_{NaCl} vs t is directly proportional to the steady-state J_W and J_S, respectively. In addition, the respective water (θ_W) and salt (θ_S) time lags are the intercepts of the linear portion of the $m_{D,\mathrm{cor}}$ vs t (or $m_{F,\mathrm{cor}}$ vs t) and m_{NaCl} vs t plots with the t-axis, where the t-axis corresponds to $m_{D,\mathrm{cor}} = m_{F,\mathrm{cor}} = 0$ and $m_{\mathrm{NaCl}} = 0$ [19]. Recognizing that θ_W based on the $m_{D,\mathrm{cor}}$ and $m_{F,\mathrm{cor}}$ should be the same helped to correct for a step-change in the mass of the feed and draw solutions at the initiation of the experiment, which is not due to the water transport across the membrane [19].

2.4 **Results and discussion**

2.4.1 Membrane cleaning results

Two membrane coupons cut from the commercial low-pressure RO TFC membrane were used in this work. Each coupon was used in 18 tests, and between the tests, the coupon and the entire system were cleaned to remove residuals of NaCl (draw solute). The first membrane was cleaned using only distilled water, while the second membrane was first cleaned using distilled water, followed by cleaning with DI water. The cleaning progress was assessed by the final conductivity in the feed (Fig. 2.3) and draw (Fig. 2.4) containers at the end of each cleaning run.

Fig. 2.3 presents the example of the progress of the cleaning process of Membrane 1 (Fig. 2.3a) and Membrane 2 (Fig. 2.3b) based on the conductivity in the feed container after 1 mol/L draw solution in the AL-DS orientation. Fig. 2.4 presents the progress of the cleaning process after the same experiment based on the conductivity in the draw container. As expected, the conductivity in both containers decreased very rapidly in the first 3-4 cleaning runs, followed by a more gradual decrease in the conductivity. In addition, as expected, the conductivities in the initial cleaning runs in the draw solution tank (Fig. 2.4) were much higher than in the feed solution tank (Fig. 2.3). However, after 20 cleaning cycles in the feed and the draw tanks, the final conductivities were the same for a given membrane. These final conductivities were around 100 μS/cm for the first membrane and 60 μS/cm for the second membrane. The difference is due to the lower conductivity of the DI water compared to the distilled water. It is important to note that the respective conductivities of the DI and distilled water are smaller than 100 and 60 μS/cm, suggesting that despite reaching (or approaching) plateaus in Figs. 2.3 and 2.4, some traces of NaCl remained in the system, most likely trapped in the membrane structure. It is possible that increasing the time of the cleaning runs and/or increasing the number of runs would bring the final conductivities closer to the respective values of the DI (5 μS/cm) and distilled water (30 μS/cm). However, we stopped the cleaning process when the conductivities in the draw and feed containers dropped to similar values in this work. The T-C meter measured the conductivity in μS/cm; however, to be more practical in the graphical representation of the cleaning process (Figs. 2.3 and 2.4), the concentration is presented in mS/cm.

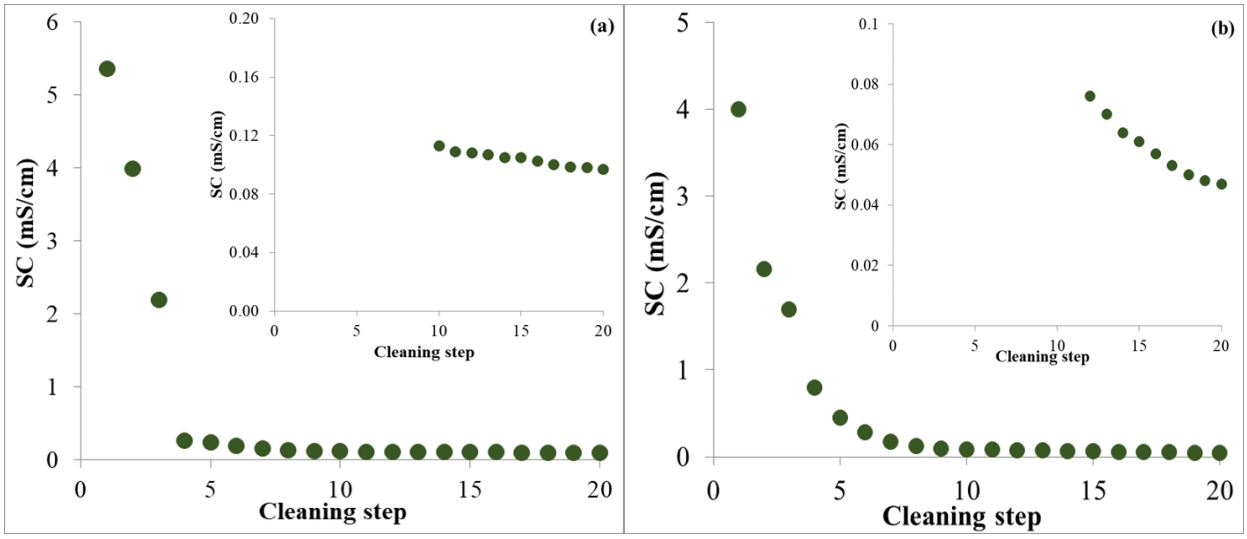

Figure 2.3 Progress of cleaning of (a) Membrane 1 and (b) Membrane 2 based on monitoring the conductivity in the feed solution container. The cleaning process presented in these figures is an example from a test performed for the AL-DS orientation and with a draw solution of 1 mol/L.

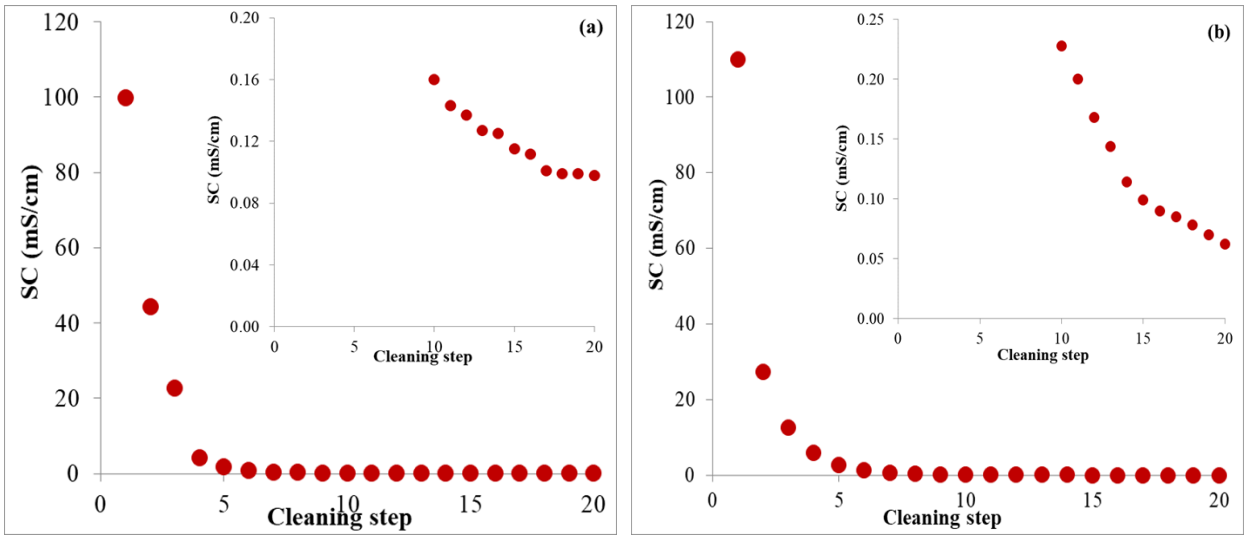

Figure 2.4 Progress of cleaning of (a) Membrane 1 and (b) Membrane 2 based on monitoring the conductivity in the draw solution container. The cleaning process presented in these figures is an example from a test performed for the AL-DS orientation anf with a draw solution of 1 mol/L.

2.4.2 Effect of membrane orientation

Figure 2.5 presents the progress of a dynamic FO experiment with Membrane (2) in the AL-DS orientation with a 2 mol/L draw solution. Fig. 2.5a presents the corrected mass of the draw and feed solutions as a function of time and the corresponding total mass. The corrected total mass is equal to zero at any time. The initial masses of the respective solutions were approximately 400 g (feed) and 700 g (draw). However, they were normalized to be zero at the beginning of the experiment (t = 0). To ensure reaching steady state, the experiment was carried out for 30 min following the initiation of the step change in the draw solution concentration. Fig. 2.5b presents the corresponding change in the mass of NaCl in the feed solution. The straight lines in both figures signify the steady-state conditions. These straight lines are extrapolated to the time axis to evaluate the respective time lags.

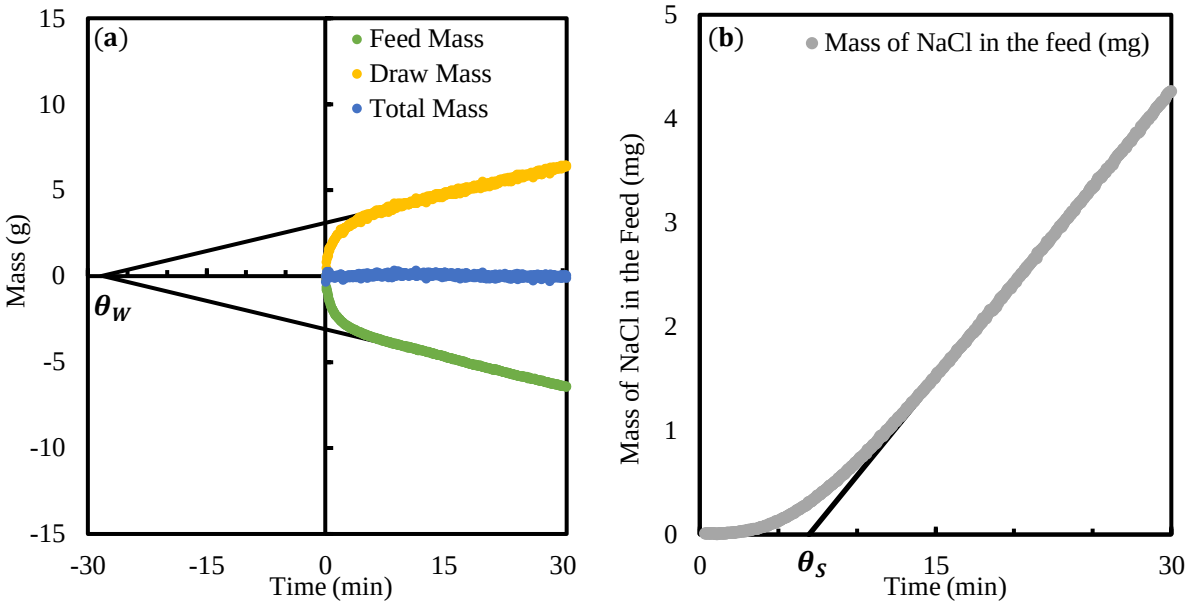

Figure 2.5. Progress of the dynamic experiment with Membrane 2 (test run #2) in the AL-DS orientation. The experiment was initiated by the step change in the draw solution concentration from 0 to 2 mol/L.

It is evident from Fig. 2.5a that the highest rate of water flux, i.e. the slope of $m(t)$, occurs immediately after initiation of the experiment. It gradually decreases until becoming constant, after approximately 10 minutes. On the other hand, the rate of the salt flux is zero in the first couple of minutes, after which it gradually increases until reaching a constant value at 10-15 minutes from the beginning of the experiment. The straight lines in Fig. 2.5 represent the respective linear regressions of the data collected between 20 min and 30 min, i.e. when the system was clearly at a steady state. The corresponding steady-state water fluxes of the draw and feed solutions are 3.18 and -3.21 L/m^2 × h and NaCl is 5.40 g/m^2 × h. The negative water flux of the feed solution indicates that water is transported from the feed side to the draw side of the membrane.

In addition to the steady-state fluxes, linear regression lines in Fig. 2.5 allow determining the time lags associated with water and salt transport across the membrane, respectively. For the water transport based on the draw and feed side, they are -28.34 min and -28.06 min. In principle, these time lags should be the same. However, compared to the magnitude of the water time lags, this difference is not significant. The negative time lag associated with water transport is associated with a positive time lag of salt of 6.95 min. The curves in Fig. 2.5 resemble those observed by Bai et al. [19] for the same membrane configuration.

Fig. 2.6 presents a dynamic FO experiment (2 mol/L) with Membrane 2 in the AL-FS orientation. The only difference between the experiments depicted in Figs. 2.5 and 2.6 are the membrane orientation.

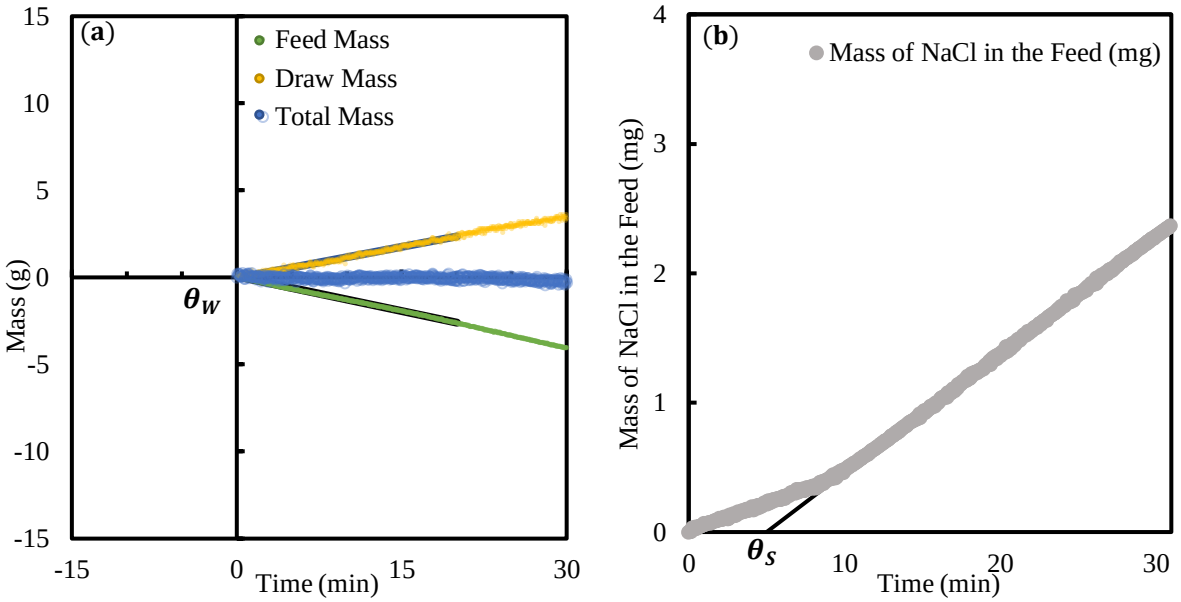

Figure 2.6. Progress of the dynamic experiment with Membrane (2) (test run #2) in the AL-FS orientation. The experiment was initiated by the step change in the draw solution concentration from 0 to 2 mol/L.

The behaviour of the membrane during the experiment with the AL-DS orientation (Fig. 2.5) appears to be very different from that with the AL-FS orientation (Fig. 2.6). There is practically no transient period in water transfer across the membrane in the latter orientation; the rate of mass loss at the feed side and the mass gain at the draw side appear constant right from the beginning of the experiment. The water fluxes based on the mass loss at the feed side and the mass gain at the draw side determined using the time frame from 10 min to 20 min, are -3.87 L/m^2 × h and 3.48 L/m^2 × h, respectively, or the average water flux is 3.67 L/m^2 × h. Therefore, the water flux in the AL-FS orientation is slightly greater than in the AL-DS orientation. In general, the opposite effect of membrane orientation on the flux is reported (higher water flux in the AL-DS orientation) [20-25] but not always [9],[26-28]. It is important to note that although there is practically no transient period in Fig. 2.6, the respective water fluxes were determined using the linear regression of the data from 10 to 20 min for AL-FS. No transient period implies zero time lag of water. In reality, there is a small water time lag of 0.38 min in Fig. 2.6a. However, in the repeated experiments, different small values (positive or negative) were observed. Therefore, we

concluded that although the water time lag might exist in the AL-FS orientation, the current resolution of the system and uncertainties associated with the processing of the raw experimental data do not allow us to report it with confidence.

Interestingly, despite no apparent dynamics in the water transport, there appears to be a dynamic behaviour associated with the reverse salt transport in Fig. 2.6b. However, it is different than in the AL-DS orientation (Fig. 2.5b). Right after the initiation of the experiment, there is a constant salt flux of 1.26 g/m^2 h during the first 9 minutes of the experiment. It is followed by a transition to a higher flux of 2.67 g/m^2 h, which prevails until the end of the experiment (30 min). It is important to note that the final reverse salt flux in the AL-FS orientation is just half of the reverse salt flux in the AL-DS orientation. The performance of FO membranes is often evaluated by the ratio of the water and the reverse salt fluxes. Using this consideration, the performance in the AL-FS orientation of the membrane investigated in this work is superior to that in the AL-DS orientation. This observation is consistent with Bai and Kruczek [28] and other works in the literature [29]. Extrapolating the final reverse salt flux to the time axis leads to the salt time lag of 5 min, which is almost two minutes less than in the AL-DS orientation.

According to Bai and Kruczek [28], the absence of dynamic behaviour in water transport in the AL-FS orientation is a consequence of defects in the active layer of the TFC membrane. The active layer has two parallel processes: diffusion across the nonporous film and diffusion across the defects. The concentration gradient drives the former within the nonporous film and the latter by the concentration gradient within a solution entrapped in the defects. The resistance to diffusion in the nonporous layer is much greater than the resistance to diffusion in the defects. Since the membrane had been saturated with water before the initiation of the experiment, the water transport across the selective layer can be approximated as a convective flow driven by the osmotic pressure gradient. Moreover, since water is incompressible, the flow across the selective layer has to be equal to the flow through the porous sublayer at any given time in both transient and steady-state periods. On the other hand, at a given time during the transient period, the rate of salt transfer depends on the position within the membrane. Due to restriction to mixing, the transport of solute in the porous sublayer is limited to diffusion, or more specifically, to diffusion plus convection; thus, internal concentration polarization exists in the porous sublayer.

Considering dynamic tests in the AL-DS orientation (Fig. 2.5), the concentrated draw solution instantly contacts the selective layer following the step change. In contrast, the other side of the selective layer is exposed to DI water. Therefore, immediately after the initiation of the experiment, there is the highest osmotic pressure gradient across the selective layer and hence the maximum water flux. At the same time, the salt starts to diffuse through the nonporous part and the defects in the selective layer. Once the salt appears at the other side of the selective layer, the osmotic pressure gradient decreases, leading to a decrease in the water flux, evident in Fig. 2.5a. At the same time, the salt starts to diffuse towards the feed solution against the water flow. This is why; there is a certain period in Fig. 2.5b during which the solute is not detected in the feed solution, whereas the water flux continuously decreases in Fig 2.5a. In this period, the salt concentration in the porous sublayer is in contact with the selective layer and the concentration profile in the pores of the sublayer layer is developing. Once a constant concentration profile in the porous sublayer is developed, the rate of solute transport becomes constant, which according to Fig. 2.5b, occurs approximately 10 minutes from the initiation of the experiment [28].

The presence of defects in the active layer is not immediately apparent in Fig. 2.5. However, assuming that resistance to salt diffusion in the nonporous layer is not negligible, it would take some time before the solute appears on the other side of the selective layer. In other words, the water flux would be constant for some time after the initiation of the experiment. On the other hand, the water flux decreases rapidly right after the initiation of the experiment, which suggests the existence of some defects, which allow leakage of the draw solution through the selective layer.

The defects in the selective layer are more evident by considering the dynamic behaviour in the AL-FS orientation. As shown in Fig. 2.6a, the water flux appears to be constant right after the initiation of the experiment. Although the free volume of the porous sublayer is filled with DI water before the initiation of the experiment, the draw solution makes contact with the selective layer almost instantaneously after the step change. A nearly constant salt concentration in contact with the selective layer is likely established very quickly. The first constant slope with the origin at $t = 0$ in Fig. 2.6b supports this hypothesis. If there were only one diffusion path for salt, the salt flux would be constant throughout the experiment. However, it is not the case in Fig. 2.6b. Between 9-10 minutes from the initiation of the experiment, the slope in Fig. 2.6b changes to a new higher

value. This can be attributed to solute diffusing through the non-defective part of the selective layer reaching the other side of the membrane. In other words, the first constant slope in Fig. 2.6b can be attributed to the leakage of the draw solution through the selective layer of the membrane, and the difference between the final slope and the initial slope on Fig. 2.6b corresponds to the diffusion of the salt through a non-defective part of the selective layer.

2.4.3 Effect of concentration of the draw solution in both orientations

Tables 2.1 and 2.2 summarize all experimental results obtained with Membranes 1 and 2, respectively. The water time lag in the AL-FS orientation is reported as zero in both tables. However, the water time lag in this orientation was not precisely zero, but it ranged within -1 min to 1 min. There was no clear trend with the concentration of the draw solution. Therefore, we attributed zero water time lags in the AL-FS orientation to the limited resolution of the system and the uncertainty resulting from the processing of the experimental data. In general, all other parameters listed in Tables 2.1 and 2.2 increase with the concentration of the draw solution. The effect of the draw solution concentration on the water flux and the reverse salt flux in both membrane orientations is presented in Figs. 2.7 and 2.8 to visualize these trends better.

Table 2.1 Summary of dynamic experiments with Membrane 1. (Toray low/pressure RO TFC membranes at 25 ± 0.3 °C). The effect of the draw solution concentration in AL-DS and AL-FS membrane orientation.

Membrane Orientation	**Draw solution concentration (mol/L)**	**Test Run**	**Water transport**		**Salt transport**	
			Flux[1] (L/m^2 h)	**Time Lag[1]** (min)	**Flux** (g/m^2 h)	**Time Lag** (min)
AL-DS	1	1	4.09	-10.51	3.31	4.03
		2	3.97	-11.18	3.73	3.99
		3	3.83	-12.27	3.66	4.01
		Average	**3.96**	**-11.32**	**3.57**	**4.01**
AL-FS		1	4.32	0	2.5	4.01
		2	3.91	0	2.38	3.10
		3	3.62	0	2.5	4.74
		Average	**3.95**	**0**	**2.46**	**3.95**
AL-DS	2	1	4.94	-24.31	3.62	6.82
		2	5.03	-22.76	3.44	6.62
		3	4.97	-22.84	3.39	7.14
		Average	**4.98**	**-23.30**	**3.48**	**6.86**
AL-FS		1	5.11	0	2.50	4.32
		2	5.17	0	2.67	4.81
		3	5.54	0	2.83	4.29
		Average	**5.27**	**0**	**2.67**	**4.48**
AL-DS	4	1	5.19	-35.65	4.83	9.99
		2	5.63	-34.27	5.03	10.01
		3	5.64	-26.71	5.01	10.59
		Average	**5.49**	**-32.21**	**4.96**	**10.20**
AL-FS		1	4.34	0	5.00	6.25
		2	4.93	0	5.15	5.43
		3	4.75	0	3.64	4.69
		Average	**4.68**	**0**	**4.60**	**5.45**

[1] Average from the respective values based on water loss in the feed solution and water gain in the draw solution.
[2] The water time lag in the AL-FS orientation was assumed to be zero.

Table 2.2. Summary of dynamic experiments with Membrane 2. (Toray low/pressure RO TFC membranes at 25 ± 0.3 °C). The effect of the draw solution concentration in AL-DS and AL-FS membrane orientation.

Membrane Orientation	Draw solution concentration (mol/L)	Test Run	Water transport		Salt transport	
			Flux[1] (L/m^2 h)	Time Lag[1] (min)	Flux (g/m^2 h)	Time Lag (min)
AL-DS	1	1	2.63	-18.62	3.72	4.82
		2	2.45	-19.38	3.74	3.87
		3	2.65	-18.95	3.82	4.67
		Average	**2.58**	**-18.98**	**3.76**	**4.45**
AL-FS		1	3.34	0	2.09	4.54
		2	3.08	0	2.39	2.96
		3	4.49	0	2.21	5.38
		Average	**3.64**	**0**	**2.23**	**4.29**
AL-DS	2	1	3.57	-30.71	5.64	6.94
		2	3.2	-28.20	5.40	6.95
		3	3.04	-25.64	5.43	6.57
		Average	**3.27**	**-28.18**	**5.49**	**6.82**
AL-FS		1	4.76	0	2.90	4.88
		2	3.87	0	2.93	5;00
		3	3.41	0	2.95	4.15
		Average	**4.01**	**0**	**2.93**	**4.68**
AL-DS	4	1	3.75	-32.58	7.58	9.17
		2	3.72	-27.93	7.74	8.83
		3	3.68	-39.31	7.91	8.58
		Average	**3.72**	**-33.27**	**7.74**	**8.86**
AL-FS		1	4.41	0	4.50	5.04
		2	4.78	0	5.16	5.50
		3	4.66	0	3.65	4.01
		Average	**4.62**	**0**	**4.44**	**4.85**

[1] Average from the respective values based on water loss in the feed solution and water gain in the draw solution.
[2] The water time lag in the AL-FS orientation was assumed to be zero.

Considering the average water and reverse salt fluxes in Figs. 2.7 and 2.8, the increasing trend with the concentration of the draw solution is more apparent for Membrane 2 than Membrane 1. J_w of Membrane 1 in the AL-FS orientation at the draw solution concentration of 2 mol/L is higher than at 4 mol/L. As the concentration of the draw solution increases, regardless of the membrane

orientation, the osmotic pressure gradient should increase, thus increasing the water flux. Also, the J_s of Membrane 1 in the AL-DS orientation at 2 mol/L is less than 1 mol/L despite a greater driving force for the reverse salt flux. It is interesting to note that these two outliers from the expected trends are observed for Membrane 1 but not for Membrane 2. As previously noted, the final cleaning steps of Membrane 2 were performed using DI water instead of distilled water for Membrane 2. This helped to achieve a lower conductivity at the end of the final wash for Membrane 2 than for Membrane 1, indicating the presence of less residual NaCl at the beginning of each experiment with Membrane 2 compared to Membrane 1. It is, therefore, possible that incomplete removal of the residual draw solute from the membrane might be responsible for the outliers in Figs. 2.7 and 2.8.

Excluding the two outliers discussed above, it is essential to indicate that the increase in J_w and J_s is not directly proportional to the concentration of the draw solution. More specifically, doubling the draw solution concentration increases J_w and J_s, but by a generally much smaller factor than 2. This observation is consistent with that of Bai and Kruczek [28]. The same applies to the water time lag in the AL-DS orientation and the salt time lag in both orientations. As the time lag (water or salt) increases, the resistance to the transport of the species increases. It might be why doubling the driving force does not lead to a doubling of J_w and J_s. A similar effect of the concentration of the draw solution on J_w and J_s was reported in the literature [15-16],[26],[29-30]. Knowing the respective time lags provides for the first time more insight on such a low increase in these fluxes with the concentration of the draw solution. Of course, the exception is the water flux in the AL-FS orientation, for which, as discussed above, we could not measure any significant time lag of water with the current resolution of the system.

The results in Tables 2.1 and 2.2, some of which are presented in Figs. 2.7 and 2.8 confirm the effect of membrane orientation discussed in the previous section. J_w in the AL-FS orientation is higher for a given concentration of the draw solution, while J_s is smaller than the corresponding J_w and J_s in the AL-DS orientation. In other words, the membrane shows a better FO performance in the AL-FS orientation and the AL-DS orientation. Also, for a given concentration of the draw solution, the salt time lag in the AL-DS orientation is higher than in the AL-FS orientation and more responsive to the changes in the draw solution concentration.

One of the motivations of this work was the variation in properties from coupon to a coupon of the same commercial membrane, which influences the trends such as the effects of draw solution concentration and membrane orientation. It is evident that except for Fig. 2.8b, the properties of Membrane 1 and Membrane 2 differ. Some comparable performance of Membranes 1 and 2 in Figs 2.7b and 2.8a at some draw solution concentrations is likely due to the previously discussed outliers in the performance of Membrane 1. In other words, the results shown in Figs. 2.7 and 2.8 confirm the hypothesis properties variation from coupon to coupon and the importance of properly cleaning the system and membrane in between the tests.

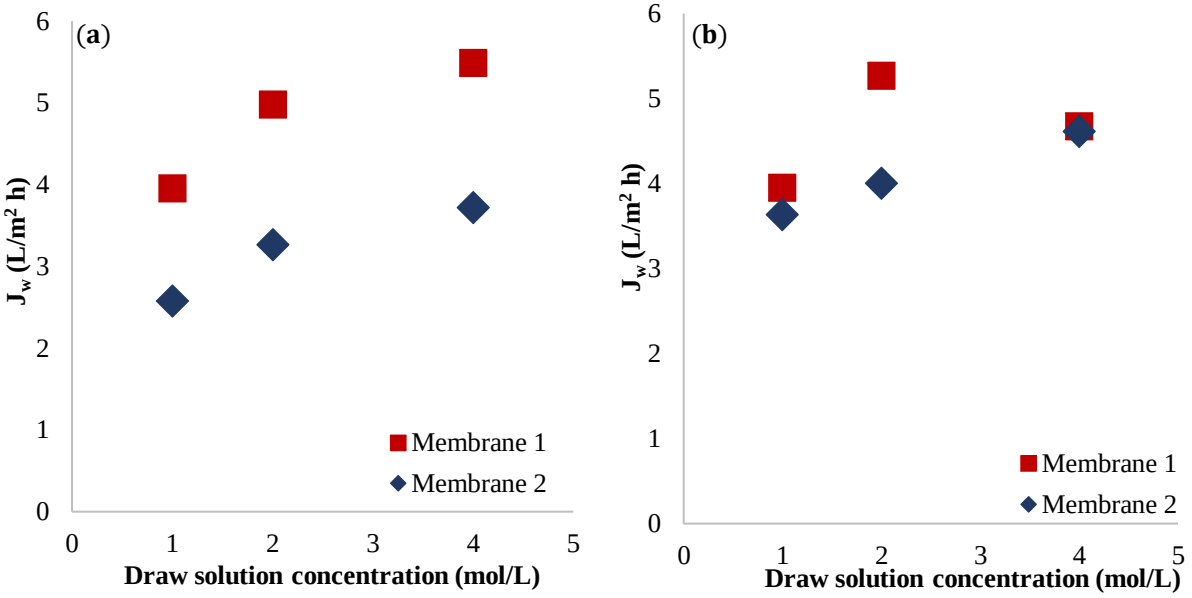

Figure 2.7 Effect of the draw solution concentration on the water flux in (a) AL-DS and (b) AL-FS membrane orientations. Each data point represents the average from three experiments using the same membrane coupon.

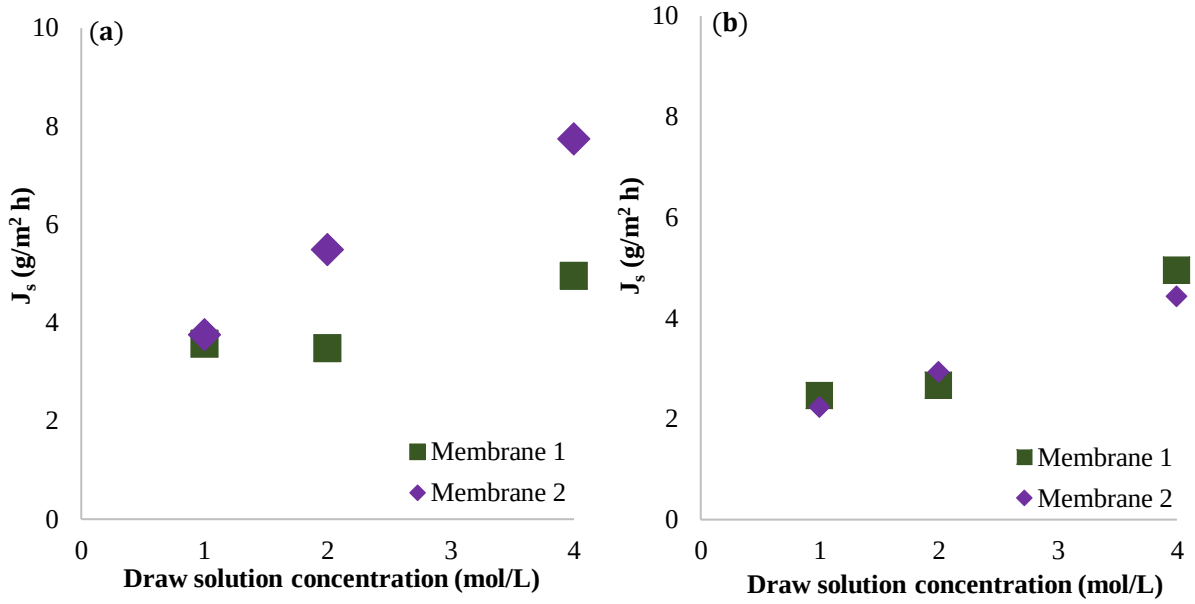

Figure 2.8 Effect of the draw solution concentration on the reverse salt flux in (a) AL-DS and (b) AL-FS membrane orientations. Each data point represents the average from three experiments using the same membrane coupon.

2.4.4 Effect of membrane cleaning on the variation in membrane performance

Considering the expected trends of the draw solution concentration on the membrane performance (Tables 2.1, 2.2 and Figs. 2.7, 2.8), using DI water instead of distilled water in the final membrane cleaning steps is beneficial for the quality of the experimental results. Another metrics to assess the quality of the experimental results is to compare the repeatability of the membrane performance by considering the standard deviations for a given condition. For Membranes 1 and 2, each experiment was repeated three times, similar to our previous work [28]. However, in our previous work, we used different coupons in the repeated experiments. Table 2.3 reports the different average performance parameters and the standard deviations for Membranes 1 and 2 and the corresponding values reported previously by Bai and Kruczek [28]. For the AL-FS orientation, we do not report the water time lag because the current resolution of the system does not allow measuring this parameter for the commercial membrane investigated in this thesis. It is important to note that Bai and Kruczek [28] reported the water time lags in the AL-FS orientation. Still, their values oscillated between -1 to 1 min without any clear trend with the concentration of the draw solution.

Table 2.3 Comparison of the average experimentally measured parameters and their standard deviations of Membranes 1 and 2 with the corresponding values reported in Ref. [21].

Orientation	Parameter	Draw solution concentration (mol/L)	Membrane		
			1	2	Ref. [21]
AL-DS	J_w [L/m^2 h]	1	3.96 ± 0.10	2.58 ± 0.04	5.23 ± 1.10
		2	4.98 ± 0.04	3.27 ± 0.22	5.42 ± 0.78
		4	5.49 ± 0.21	3.72 ± 0.08	6.45 ± 0.64
	θ_W [min]	1	-11.32 ± 0.73	-18.98 ± 0.45	-11.11 ± 2.48
		2	-23.30 ± 0.71	-28.18 ± 2.07	-18.42 ± 5.49
		4	-32.21 ± 3.93	-33.27 ± 4.67	-19.83 ± 4.61
	J_s [g/m^2 h]	1	3.57 ± 0.18	3.76 ± 0.05	6.13 ± 0.70
		2	3.48 ± 0.10	5.49 ± 0.11	9.35 ± 2.53
		4	4.96 ± 0.09	7.74 ± 0.13	16.58 ± 7.39
	θ_S [min]	1	4.01 ± 0.01	4.45 ± 0.42	3.69 ± 0.42
		2	6.86 ± 0.21	6.82 ± 0.18	5.49 ± 1.80
		4	10.20 ± 0.28	8.86 ± 0.24	5.76 ± 2.39
AL-FS	J_w [L/m^2 h]	1	3.95 ± 0.28	3.64 ± 0.62	3.98 ± 0.23
		2	5.27 ± 0.19	4.01 ± 0.56	4.24 ± 0.37
		4	4.68 ± 0.25	4.62 ± 0.21	5.62 ± 0.20
	J_s [g/m^2 h]	1	2.46 ± 0.25	2.23 ± 0.34	1.96 ± 0.26
		2	2.67 ± 0.08	2.93 ± 0.08	2.63 ± 0.09
		4	4.60 ± 0.72	4.44 ± 0.18	3.92 ± 0.64
	θ_S [min]	1	3.95 ± 0.67	4.29 ± 1.01	4.18 ± 1.00
		2	4.48 ± 0.24	4.68 ± 0.38	4.68 ± 0.39
		4	5.45 ± 0.64	4.85 ± 0.52	4.28 ± 0.41

Considering the standard deviations reported in Table 2.3, it appears that the membrane cleaning reduces the variability of the parameters determined in the AL-DS orientation. On the other hand, there is no apparent effect for the parameters determined in the AL-FS orientation. The standard deviations observed when cleaning the membrane to generate repeated values are comparable to those when a different coupon is used in each repeated run. Comparing the standard deviations for Membranes 1 and 2, there appears to be no advantage of using DI water in the final steps instead of the distilled water. For some parameters, the standard deviations associated with

Membrane 1 are even lower than with Membrane 2. In other words, the anticipated advantage of using the DI water in the final cleaning steps is not confirmed based on the respective standard deviations.

2.5 Conclusions

In pursuit of generating reliable experimental data for modelling the transport of water and draw solute in commercial low-pressure RO membrane tested in dynamic forward experiments, we used the same membrane at all experimental conditions. The membrane was extensively washed in-situ between each experiment using two slightly different protocols. Each protocol used 20 cleaning steps with fresh water in each step. Distilled water was used in the first 10 steps in both protocols, and we continued using fresh distilled water in the remaining 10 steps in the first protocol and deionized water in the second protocol. In both protocols, the same conductivity was eventually reached at the feed and the draw sides of the membrane after the final cleaning step. The final conductivity when using deionized water was lower than when using distilled water. However, in both cases, the final conductivity was higher than the respective conductivities of the distilled water and deionized water.

When using the deionized water in the final steps, the observed effect of the draw solution concentration on different transport parameters followed the expected trends. On the other hand, when using distilled water in all steps, the expected trends were not fully reproduced. However, better adherence to the expected trends when using deionized water in the final cleaning steps did not translate to lower variation in the repeated experiments. The respective standard deviations observed in both cleaning protocols were comparable.

The current study confirmed variation in transport parameters from coupon to coupon of the same commercial membrane. As such, the need to develop the appropriate cleaning protocol remains to be an essential objective. Using more than 20 cleaning steps could help to lower the final conductivity of the washing water. Similarly, increasing the time between each step could help accomplish that too. However, these two approaches might not be practical, as they would lead to the already very long time required by both protocols. Instead, it might be advantageous to use washing water at a higher temperature. It would facilitate desorption of the draw solute from the membrane and the system and reduce the total cleaning time.

2.6 Nomenclature

A	Water permeance	L/m^2 h bar
a	Correction factor	-
B	Salt permeability	g/m^2 h
C_1	In the AL-DS orientation, it represents the salt concentration in the bulk draw solution. In the AL-FS, it represents the salt concentration in the bulk feed solution.	mol/L
C_2	In the AL-DS orientation, it represents the salt concentration in the membrane surface at the active layer side towards the draw solution. In the AL-FS orientation, it represents the salt concentration in the membrane surface at the active layer side towards the feed solution.	mol/L
C_3	In the AL-DS and AL-FS orientations, it represents the salt concentration inside the membrane at the interface between the active layer and the porous support.	mol/L
C_4	In the AL-DS orientation, it represents the salt concentration in the membrane surface at the porous support layer side towards the feed solution. In the AL-FS orientation, it represents the salt concentration in the membrane surface at the porous support layer side towards the draw solution.	mol/L
C_5	In the AL-DS orientation, it represents the salt concentration in the bulk feed solution. In the AL-FS orientation, it represents the salt concentration in the bulk draw solution.	mol/L
c_{NaCl}	NaCl concentration in the feed solution	mg/L
Δp	Hydraulic pressure gradient	bar
$\Delta \pi$	Osmotic pressure gradient	bar
Δc	Solute concentration gradient	mol/L
$\Delta \pi_{eff}$	Effective osmotic pressure gradient	bar
i	Dissociation factor of solutes in the solution	-
J_s	Salt flux	g/m^2 h
J_w	Water flux	L/m^2 h
m	Mass at the time "t"	mg/L
m_D	Mass of the draw solution	mg/L
m_F	Mass of the feed solution	mg/L
$m_{D,cor}$	Corrected mass of the draw solution	mg/L
$m_{F,cor}$	Corrected mass of the feed solution	mg/L
$m_{T,cor}$	Corrected total mass	mg/L
m_{NaCl}	Mass of NaCl	mg/L

R	Universal gas constant	bar L/mol K
S	Structural parameter	m
SC	Specific Conductivity	mS/cm
T	Absolute temperature	K
t	Time	min

Subscripts

D	Draw solution
F	Feed solution
S	Salt
W	Water

Greek letters

ε_{eff}	Effective porosity	-
τ	Tortuosity of the membrane	-

Abbreviations

AL-DS	Active Layer facing the Draw Solution
AL-FS	Active Layer facing the Feed Solution
CP	Concentration Polarization
DI	Deionized water
ECP	External Concentration Polarization
FO	It may refer to Forward Osmosis or to the membrane orientation in which the Active Layer is facing the Feed Solution
ICP	Internal Concentration Polarization
ODMP	Osmotically Driven Membrane Processes
PET	Polyethylene terephtalate
PRO	It may refer to Pressure Retarded Osmosis or to the membrane orientation in which the Active Layer is facing the Draw Solution
PS	Polysulfone
RO	Reverse Osmosis
TFC	Thin Film Composite Membrane
TMC	Trimesoyl Chloride
UF	Ultrafiltration

References

[1] M. Qasim, N. A. Darwish, S. Sarp, and N. Hilal, "Water desalination by forward (direct) osmosis phenomenon: A comprehensive review," *Desalination*, vol. 374, pp. 47–69, 2015.

[2] F. Nave, R. Kommalapati, and A. Thompson, "Introductory Chapter: Osmotically Driven Membrane Processes," *IntechOpen*, 2018.

[3] H. Zheng, "General Problems in Seawater Desalination," in *Solar Energy Desalination Technology*, Elsevier, 2017, pp. 1–46.

[4] J. Kucera, *Reverse Osmosis: Design, Processes, and Applications for Engineers*. Scrivener Publishing LLC, 2010.

[5] S. Yang, B. Gao, A. Jang, H. kyong Shon, and Q. Yue, "Municipal wastewater treatment by forward osmosis using seawater concentrate as draw solution," *Chemosphere*, vol. 237, p. 124485, 2019.

[6] P. Xiao, L. D. Nghiem, Y. Yin, X. Li, M. Zhang, G. Chen, J. Song, T. He, "A sacrificial-layer approach to fabricate polysulfone support for forward osmosis thin-film composite membranes with reduced internal concentration polarisation," *J. Memb. Sci.*, vol. 481, pp. 106–114, 2015.

[7] T. Y. Cath, N. T. Hancock, C. D. Lundin, C. Hoppe-Jones, and J. E. Drewes, "A multi-barrier osmotic dilution process for simultaneous desalination and purification of impaired water," *J. Memb. Sci.*, vol. 362, no. 1–2, pp. 417–426, 2010.

[8] J. R. McCutcheon, R. L. McGinnis, and M. Elimelech, "A novel ammonia-carbon dioxide forward (direct) osmosis desalination process," *Desalination*, vol. 174, no. 1, pp. 1–11, 2005.

[9] S. Zhao, L. Zou, and D. Mulcahy, "Effects of membrane orientation on process performance in forward osmosis applications," *J. Memb. Sci.*, vol. 382, no. 1–2, pp. 308–315, 2011.

[10] S. L. Loo, A. G. Fane, W. B. Krantz, and T. T. Lim, "Emergency water supply: A review of potential technologies and selection criteria," *Water Res.*, vol. 46, no. 10, pp. 3125–3151, 2012.

[11] B. D. Coday, P. Xu, E. G. Beaudry, J. Herron, K. Lampi, N. T. Hancock, T. Y. Cath, "The sweet spot of forward osmosis: Treatment of produced water, drilling wastewater, and other complex and difficult liquid streams," *Desalination*, vol. 333, no. 1, pp. 23–35, 2014.

[12] X. Wang, Y. Zhao, X. Li, and Y. Ren, "Performance evaluation of a microfiltration-osmotic membrane bioreactor (MF-OMBR) during removing silver nanoparticles from simulated wastewater," *Chem. Eng. J.*, vol. 313, pp. 171–178, 2017.

[13] M. Xie, L. D. Nghiem, W. E. Price, and M. Elimelech, "Toward Resource Recovery from Wastewater: Extraction of Phosphorus from Digested Sludge Using a Hybrid Forward Osmosis-Membrane Distillation Process," *Environ. Sci. Technol. Lett.*, vol. 1, no. 2, pp. 191–195, 2014.

[14] A. Haupt and A. Lerch, "Forward osmosis application in manufacturing industries: A short review," *Membranes (Basel).*, vol. 8, no. 3, 2018.

[15] A. Tiraferri, N. Y. Yip, A. P. Straub, S. Romero-Vargas Castrillon, and M. Elimelech, "A method for the simultaneous determination of transport and structural parameters of forward osmosis membranes," *J. Memb. Sci.*, vol. 444, pp. 523–538, 2013.

[16] J. T. Martin, G. Kolliopoulos, and V. G. Papangelakis, "An improved model for membrane characterization in forward osmosis," *J. Memb. Sci.*, vol. 598, no. November 2019, p. 117668, 2020.

[17] B. Kim, G. Gwak, and S. Hong, "Review on methodology for determining forward osmosis (FO) membrane characteristics: Water permeability (A), solute permeability (B), and structural parameter (S)," *Desalination*, vol. 422, no. December 2015, pp. 5–16, 2017.

[18] S. S. Manickam and J. R. McCutcheon, "Understanding mass transfer through asymmetric membranes during forward osmosis: A historical perspective and critical review on measuring structural parameter with semi-empirical models and characterization approaches," *Desalination*, vol. 421, pp. 110–126, 2017.

[19] D. Bai, F. Asempour, and B. Kruczek, "Can the time-lag method be used for the characterization of liquid permeation membranes?," *Chem. Eng. Res. Des.*, vol. 162, no. 2, pp. 228–237, 2020.

[20] J. R. McCutcheon and M. Elimelech, “Influence of concentrative and dilutive internal concentration polarization on flux behavior in forward osmosis,” *J. Memb. Sci.*, vol. 284, no. 1–2, pp. 237–247, 2006.

[21] D. H. Jung, J. Lee, D. Y. Kim, Y. G. Lee, M. Park, S. Lee, D. R. Yang, J. H. Kim, “Simulation of forward osmosis membrane process: Effect of membrane orientation and flow direction of feed and draw solutions,” Desalination, vol. 277, no. 1–3, pp. 83–91, 2011

[22] C. Y. Tang, Q. She, W. C. L. Lay, R. Wang, and A. G. Fane, “Coupled effects of internal concentration polarization and fouling on flux behavior of forward osmosis membranes during humic acid filtration,” J. Memb. Sci., vol. 354, no. 1–2, pp. 123–133, 2010.

[23] Q. She, X. Jin, and C. Y. Tang, “Osmotic power production from salinity gradient resource by pressure retarded osmosis: Effects of operating conditions and reverse solute diffusion,” J. Memb. Sci., vol. 401–402, pp. 262–273, 2012.

[24] H. Y. Ng, W. Tang, and W. S. Wong, “Performance of forward (direct) osmosis process: Membrane structure and transport phenomenon,” Environ. Sci. Technol., vol. 40, no. 7, pp. 2408–2413, 2006.

[25] S. Liyanaarachchi, S. Muthukumaran, J. Kaiser, P. Rogers, L. Shu, H. K. Shon f, V. Jegatheesan. “Computing the effective diffusion coefficient of solutes in a multi-salts solutions during forward osmosis (FO) membrane filtration: Experiments and mathematical modelling,” J. Environ. Manage., vol. 214, pp. 215–223, 2018.

[26] Y. Xu, X. Peng, C. Y. Tang, Q. S. Fu, and S. Nie, “Effect of draw solution concentration and operating conditions on forward osmosis and pressure retarded osmosis performance in a spiral wound module,” J. Memb. Sci., vol. 348, no. 1–2, pp. 298–309, 2010.

[27] G. T. Gray, J. R. Mccutcheon, and M. Elimelech, “Internal concentration polarization in forward osmosis " role of membrane orientation,” 2006 https://doi.org/10.1016/j.desal.2006.02.003

[28] D. Bai, B. Kruczek, Effect of membrane orientation and concertation of draw solution on behaviors of commercial low-pressure RO membrane in novel dynamic forward osmosis tests, under review in Desalination

[29] M. R. Chowdhury and J. R. McCutcheon, "Elucidating the impact of temperature gradients across membranes during forward osmosis: Coupling heat and mass transfer models for better prediction of real osmotic systems," J. Memb. Sci., vol. 553, no. December 2017, pp. 189–199, 2018.

[30] W. A. Phillip, J. S. Yong, and M. Elimelech, "Reverse draw solute permeation in forward osmosis: Modeling and experiments," *Environ. Sci. Technol.*, vol. 44, no. 13, pp. 5170–5176, 2010.

Chapter 3

Estimation of the permeability and structural parameters in thin-film composite membranes from Forward Osmosis experimental data

Sofia Reyes-Lombardo, Boguslaw Kruczek, Jules Thibault*

Department of Chemical & Biological Engineering
University of Ottawa
161 Louis Pasteur, Ottawa, ON K1N 6N5, Canada

*** To whom correspondence should be addressed.**

Chapter 3. Estimation of the permeability and structural parameters in thin-film composite membranes from Forward Osmosis experimental data.

Abstract

Forward osmosis (FO) has increased in popularity in the last decades for its many advantages and potential applications. The main limitation of FO for broader market penetration is the lack of feasible commercial membranes. The current FO research focuses on the direction to take for developing ideal membranes that will yield high water flux and low solute flux. Nowadays, thin-film composite (TFC) membranes have been shown to be the best option for FO processes. However, the thick porous support layer of TFC membranes leads to substantial internal concentration polarization (ICP) and, as a result, to lower water flux. To develop better FO membranes, it is essential to characterize each membrane using performance metrics properly. For FO membranes, three intrinsic parameters can adequately describe the performance of a membrane for a given process: active layer water permeance (A), active layer solute permeance (B) and porous layer structural parameter (S). In previous works, the characterization of TFC membranes was achieved experimentally, using a reverse osmosis system to obtain the values of A and B. Subsequently, the value of S was obtained from FO experiments. In this work, A, B and S were obtained experimentally using a FO system exclusively. These parameters were calculated from experimental data and compared using three different models, two models from the literature and one based strictly on the first Fick's law of diffusion.

3.1 Introduction

One of the focuses of forward osmosis research is the development of new membranes appropriate for FO applications. This can only be achieved with the evaluation of the intrinsic structural parameters for a given application [1]. An ideal FO membrane should have an active layer with high water permeability and perfect salt rejection on a support layer that minimizes the resistance to solute transport while having good mechanical properties and a wide range of pH tolerance [2]. Membrane performance is described by reporting the values of water flux (J_w) and reverse solute flux (J_s). However, these values depend on the experimental conditions of the system, including the concentration, often expressed in terms of osmotic pressure, of the draw and feed solutions, and the type of solute. This is not the most effective way to evaluate and compare the membrane performance, as the operating conditions will be different between each experimental data set [3].

Three intrinsic parameters, namely the water permeability coefficient of the active layer (A), the solute permeability coefficient of the active layer (B) and the structural parameter (S) of the porous support layer, can adequately describe the performance of FO membranes. Indeed, parameters A and B describe the transport of water and solute across the active layer of the membrane, whereas S represents the resistance to solute transport in the porous sublayer [3]. A, B, and S are membrane performance metrics, which can be used to compare different FO membranes. These parameters can also be used to predict water and solute flux for various experimental conditions.

The water permeability coefficient (A) is expected to be as high as possible, thus leading to higher water flux, whereas it is desired to achieve the lowest possible solute flux across the membrane, i.e. the lowest solute permeability coefficient (B). The structural parameter S of the porous support layer increases with an increase in tortuosity and decreases with an increase in the void fraction Although the structural parameter affects both water flux (J_w) and reverse solute flux (J_s), its effect is much more important on J_w as it is much greater than the J_s. The structural parameter S dictates the severity of internal concentration polarization. To decrease S, it is necessary to decrease the thickness and increase the void fraction of the porous support layer [4-5].

Currently, the standard approach to measure these parameters requires the use of two separate processes. Parameters *A* and *B* are typically measured in reverse osmosis (RO) tests by applying transmembrane hydraulic pressure. Then, the membrane is tested in an osmotically-driven process, such as FO, to estimate the support layer structural parameter (*S*). It has been shown in recent years that parameter *S* could be determined experimentally for the two possible membrane orientations. The two membrane orientations are the active layer facing the draw solution (AL-DS) and the active layer facing the feed solution (AL-FS) solution [3]. This dual-process method raises some concerns relative to its efficacy. Indeed, the high pressure used in the RO process to characterize FO membranes could damage the membranes. In addition, it is assumed that the transport parameters are transferable between RO and FO processes even though in FO, no hydraulic pressure is used, and the flux is only caused by a transmembrane difference in the osmotic pressure. Some studies have shown significant variation in the estimation of transport parameters between the results of RO and FO processes [6].

In this work, a method for characterizing TFC membranes is presented. The experimental results were obtained employing a FO lab-scale system, with three concentrations of the draw solution (1, 2 and 4 mol/L) and two membrane orientations (AL-DS and AL-FS). A set of three experimental water and salt fluxes were obtained in triplicates. The intrinsic transport parameters were estimated by non-linear regression to minimize the sum of squares between the experimental flux data and the flux predicted by a transport model. Three models, all based on the first Fick's law of diffusion, were used; two models from the literature and one developed in this work. The determination of the three intrinsic transport parameters (*A*, *B* and *S*) allows evaluating the performance of TFC membranes and may suggest some modifications to improve their performance.

3.2 Theoretical background

For the determination of the intrinsic transport parameters, namely *A*, *B* and *S*, it is necessary to fit the data obtained experimentally with the data predicted by the model developed to represent the permeation of water and salt across the TFC membrane. The three models used in this investigation were all obtained, starting with the equation of the first Fick's law of diffusion. In a typical FO experiment, the salt concentrations of the draw and feed solutions are set, and the water and salt fluxes are measured under steady state. However, the available concentration driving force, most often expressed as an osmotic pressure difference, is not entirely available to generate the water and salt fluxes across the semipermeable thin active layer because of the presence of concentration polarization (CP) on both sides of this thin active layer. CP occurs when the concentration at the membrane surface is different from the concentration of the bulk solution, thus reducing the transmembrane driving force. Since the water flux is proportional to the difference in the osmotic pressure at the interfaces of the active layer, the CP thereby reduces the flux of water. When the CP is present in the solution boundary layer adjacent to the membrane surface, it is referred to as external concentration polarization (ECP), whereas when it is present at the interface of the active layer and the porous support layer, it is referred to as internal concentration polarization (ICP). The ECP can be partly mitigated by increasing the turbulence in the boundary layer. On the other hand, the ICP occurring in the porous support layer cannot be reduced by modifying the hydrodynamic conditions of the system but could be reduced by modifying the structure of the porous layer [7]. The ICP has a greater impact on the performance of the membrane ECP and some studies have reported a reduction in water flux of as much as 80% [8].

Some models have been proposed to estimate the structural parameter and the permeability (or permeance) of water and salt of TFC membranes from experimental data. Among the most comprehensive models are those of Tiraferri et al. [3] and Martin et al. [9]. Tiraferri et al. [3] developed a model to calculate the fluxes of water and salt. This model, presented in Eqs. (3-1) and (3-2) is used to determine the water permeance *A*, the salt permeance *B* and the porous layer structural parameter *S* using non-linear least-squares regression analysis to fit the experimental water and salt fluxes. It should be noted that the terms permeability and permeance indicate two different parameters. The permeability is the thickness-normalized permeance, and since the

thickness of the active layer of the TFC membrane is typically unknown, the reported *A* and *B* are the membrane permeances. Despite this, they are commonly referred to as permeability in the pertaining literature.

Tiraferri et al. [3] assumed that the effect of ECP is negligible for the membrane in the FO mode, i.e., the mass transfer coefficient (*k*) is assumed very large and, as a result, the value of $exp\left(\frac{J_w}{k}\right) = 1$. For this reason, the mass transfer coefficient in the draw solution will not be included in these equations. The mass transfer coefficient in the draw and feed solution will not be used directly in Eqs. (3-1) and (3-2). The detailed derivation for Eqs. (3-1) and (3-2) are presented in Appendix A. Note that in these two equations, the permeance parameter is typically used because the thickness of the active layer is usually not known. The permeance is equal to the permeability divided by the thickness of the active layer of the membrane. Eq. (3-1) is an implicit equation as the expression of the water is itself a function of the water flux. In contrast, Eq. (3-2) is an explicit equation.

$$J_w = A\left\{\frac{\pi_D exp\left(-\frac{J_w S}{D}\right) - \pi_F exp\left(\frac{J_w}{k}\right)}{1 + \frac{B}{J_w}\left[exp\left(\frac{J_w}{k}\right) - exp\left(-\frac{J_w S}{D}\right)\right]}\right\} \tag{3-1}$$

$$J_s = B\left\{\frac{c_D exp\left(-\frac{J_w S}{D}\right) - c_F exp\left(\frac{J_w}{k}\right)}{1 + \frac{B}{J_w}\left[exp\left(\frac{J_w}{k}\right) - exp\left(-\frac{J_w S}{D}\right)\right]}\right\} \tag{3-2}$$

In Eqs. (3-1) and (3-2), J_w is the water flux (L/m^2 h), *A* (L/m^2 h bar) is the water permeance coefficient, *B* (L/m^2 h) is the salt permeance coefficient and *S* (m) the structural parameter of the porous layer. J_w is calculated using the osmotic pressure (bar) of the draw solution (π_D) and the feed solution (π_F). J_s is the salt flux in (mmol/m^2 h) and it is calculated using the concentrations of the draw and feed solutions (c_D and c_F) in mmol/L. *D* (m^2/h) is the diffusion coefficient of salt in the draw solution.

Martin et al. [9] derived similar equations (Eqs. (3-3) and (3-4)) for a FO membrane based on Tiraferri et al. [3] work, for which the effect of ECP is considered. Thus, the value of $exp\left(\frac{J_w}{k}\right)$ is calculated with the mass transfer coefficient on the feed solution k_f and the experimental water

flux. Since the effect of ECP in the draw solution is considered, the equations include the value for the mass transfer coefficient on this side of the membrane.

$$J_w = A\left\{\frac{\pi_D exp\left[-J_w\left(\frac{1}{k_d}+\frac{S}{D}\right)\right]-\pi_F exp\left(\frac{J_w}{k_f}\right)}{1+\frac{B}{J_w}\left\{exp\left(\frac{J_w}{k_f}\right)-exp\left[-J_w\left(\frac{1}{k_d}+\frac{S}{D}\right)\right]\right\}}\right\} \quad (3\text{-}3)$$

$$J_s = B\left\{\frac{c_D exp\left[-J_w\left(\frac{1}{k_d}+\frac{S}{D}\right)\right]-c_F exp\left(\frac{J_w}{k_f}\right)}{1+\frac{B}{J_w}\left\{exp\left(\frac{J_w}{k_f}\right)-exp\left[-J_w\left(\frac{1}{k_d}+\frac{S}{D}\right)\right]\right\}}\right\} \quad (3\text{-}4)$$

where k_d is the mass transfer coefficient in the boundary layer of the draw solution and k_f is the mass transfer coefficient on the side of the feed solution.

To use Eqs. (3-1)-(3-2) or Eqs. (3-3)-(3-4) to determine the three membrane transport parameters, namely *A*, *B* and *S*, a minimum of three experiments under different operating conditions are required. Each experiment, with known salt concentrations of the feed and draw solutions, provide the experimental fluxes of water and salt. In addition to the above two models, a third mathematical model was developed in this work, which is also based on the first Fick's law of diffusion. This model uses known mass transfer correlations to estimate the mass transfer coefficients prevailing in the two boundary layers. In addition, this model serves to explore the impact of different parameters of the membrane. This model was developed with the assumption that the thicknesses of the two boundary layers, the active layer and the porous layer, are known. With this model and the assumed geometrical characteristics of the membrane, it can estimate the values of *A* and *B* for each experiment.

3.3 Methodology

The experimental data was obtained using the FO system schematically presented in Figure 3.1. The FO system is described in detail elsewhere (Reyes et al. 2021) [15].

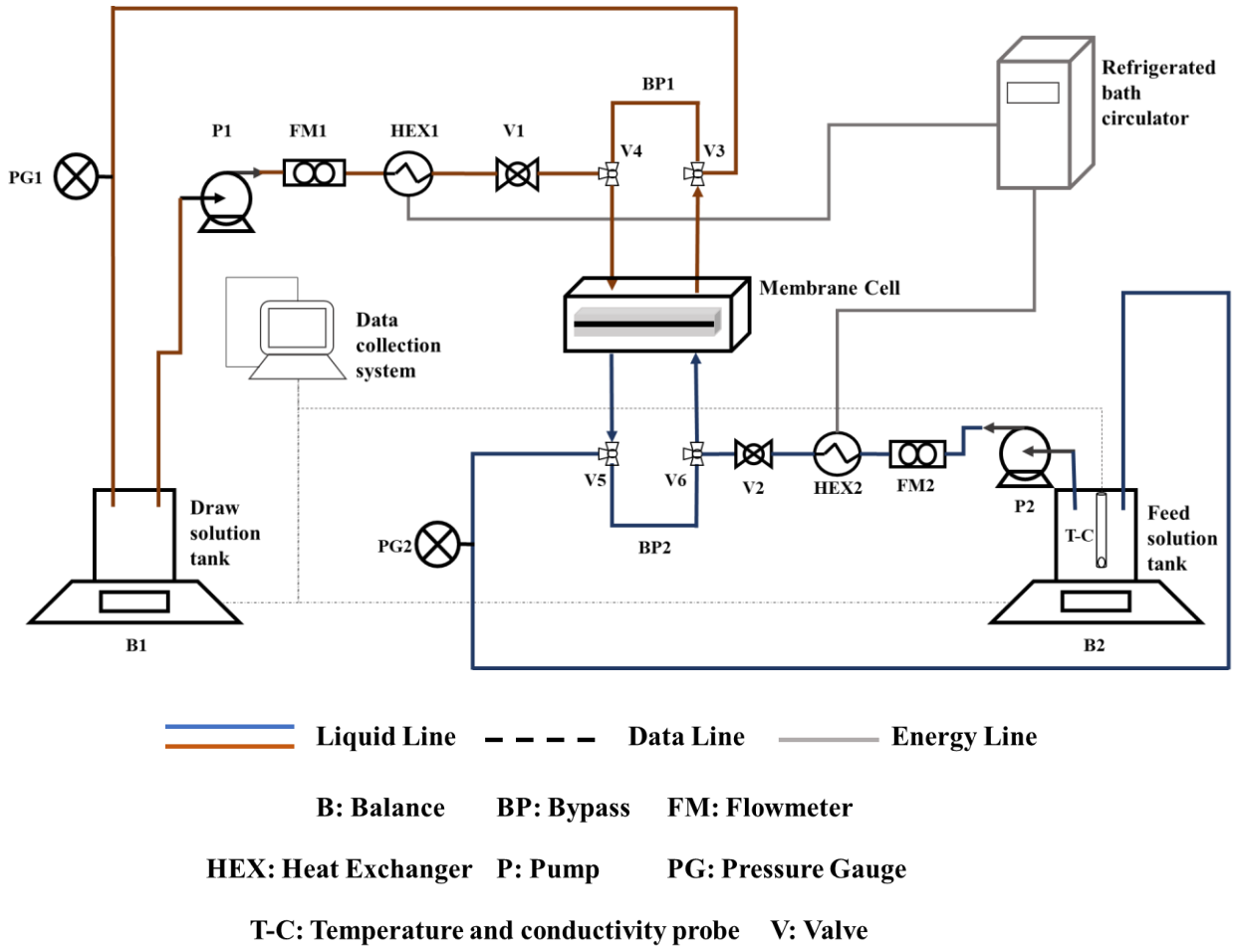

Figure 3.1 Schematic diagram of the Forward Osmosis testing system [10].

Three sets of experimental data were used in this work. Two sets of results from Reyes et al. [15] work, in which a single TFC membrane coupon was tested in the AL-FS (active layer facing the feed solution) and AL-DS (active layer facing the draw solution) membrane orientations in the FO lab-scale system, were used and denoted as the Membrane 1 and Membrane 2. These results of each set of experiments were obtained with the same membrane, which implies that, between two experiments, the membrane system was thoroughly cleaned using deionized distilled water. The third set of experimental data was obtained by Bai and Kruczek [16] using the same experimental system and the same type of TFC membranes with the exception that a new membrane coupon was used for each experiment. For each set of data, 18 experiments were performed: triplicate experiments for three different salt concentrations for both AL-DS and AL-FS. The summary of all these experimental results is presented in Tables 3.1 and 3.2.

To validate the accuracy of the mass transfer models used in this work, similar data reported in the literature was used to estimate the values of *A*, *B* and *S* and were compared with those reported by the same authors [3],[9]. A sensitivity analysis of the three models was also performed with respect to the intrinsic transport parameters. Transport parameters *A*, *B* and *S* were modified by increasing and decreasing their values by 10% to 50%. This analysis allowed observing the impact and sensitivity of each parameter on the water and salt fluxes.

Table 3.1 Experimental data for the TFC membrane in the AL-DS and AL-FS orientation.

Orientation	**Parameter**	**Draw solution concentration (mol/L)**	**Membrane**		
			1	**2**	**Ref. [16][1]**
AL-DS	J_w [L/m^{2}h]	1	3.96 ± 0.10	2.58 ± 0.04	5.23 ± 1.10
		2	4.98 ± 0.04	3.27 ± 0.22	5.42 ± 0.78
		4	5.49 ± 0.21	3.72 ± 0.08	6.45 ± 0.64
	J_s [g/m^{2}h]	1	3.57 ± 0.18	3.76 ± 0.05	6.13 ± 0.70
		2	3.48 ± 0.10	5.49 ± 0.11	9.35 ± 2.53
		4	4.96 ± 0.09	7.74 ± 0.13	16.58 ± 7.39
AL-FS	J_w [L/m^{2}h]	1	3.95 ± 0.28	3.64 ± 0.62	3.98 ± 0.23
		2	5.27 ± 0.19	4.01 ± 0.56	4.24 ± 0.37
		4	4.68 ± 0.25	4.62 ± 0.21	5.62 ± 0.20
	J_s [g/m^{2}h]	1	2.46 ± 0.25	2.23 ± 0.34	1.96 ± 0.26
		2	2.67 ± 0.08	2.93 ± 0.08	2.63 ± 0.09
		4	4.60 ± 0.72	4.44 ± 0.18	3.92 ± 0.64

1 Ref. [16] Bai and Kruczek.

3.3.1 Physical properties of the NaCl aqueous solutions.

The physical properties of NaCl solutions were calculated as follows. Djebedjian et al. [11] have suggested numerous equations to calculate the properties of the NaCl solutions. The osmotic pressure was calculated using the correlations provided by Martin et al. [9] and by Tiraferri et al. [3]. These two sets of values of the osmotic pressure for NaCl solutions are presented in Table 3.5. As seen in Table 3.5, the two values are similar. The correlation provided by Martin et al. [9] will be used in the investigation.

$$\pi = X_{1,\pi}C^2 + X_{2,\pi}C \qquad 3\text{-}5$$

with $X_{1,\pi} = 6.42$, $X_{2,\pi} = 39.26$, and the concentration C is expressed in mol/L.

Table 3.2 Osmotic pressure values obtained from Tiraferri et al. [3] and Martin et al. [9].

Draw Solution (mol/L)	**π_{NaCl} (bar)**	
	Tiraferri et al. (2013)	Martin et al. (2020)
1	49.55	45.68
2	99.11	104.20
4	198.22	259.76

The density ρ (kg/m^3), dynamic viscosity μ (kg/m s) and kinematic viscosity ν (m^2/s) were calculated using Eqs. (3-6)-(3-9), provided by Djebedjian et al. [11]:

$$\rho = 498.4m + \sqrt{248400m^2 + 752.4mC} \qquad (3\text{-}6)$$

where C is the concentration of the NaCl solution in kg/m^3 and m is a parameter calculated using Eq. (2-7).

$$m = 1.0069 - 2.757x10^{-4}T \qquad (3\text{-}7)$$

$$\mu = 1.234X10^{-6}exp\left(0.00212C + \frac{1965}{273.15 + T}\right) \qquad (3\text{-}8)$$

$$v = \frac{\mu}{\rho} \qquad (3\text{-}9)$$

The diffusion coefficient of NaCl in an aqueous solution was calculated using Eq. (3-10) provided by Djebedjian et al. [11].

$$D = 6.725x10^{-6}exp\left(0.1546x10^{-3}C - \frac{2513}{273.15+T}\right) \quad (3\text{-}10)$$

The mass transfer coefficient was estimated using a correlation giving the Sherwood number as a function of the Reynolds and Schmidt numbers [12]. The variable v_∞ is the estimated fluid velocity of the solution in the membrane test cell.

$$Re = \frac{v_\infty L}{v} \quad (3\text{-}11)$$

$$Sc = \frac{v}{D} \quad (3\text{-}12)$$

$$Sh = 0.08Re_L^{0.875}Sc^{0.25} \quad (3\text{-}13)$$

$$k_c = \frac{ShD}{L} \quad (3\text{-}14)$$

where L is the characteristic length of the respective channel of the membrane test cell.

3.4 Results and discussion

The calculated values for *A*, *B* and *S* obtained by fitting the three sets of experimental data with the models of Tiraferri et al. [3] and Martin et al. [9] are presented in Table 3.3 for the TFC membrane in the AL-FS orientation and Table 3.4 for the membrane in AL-DS with no hydraulic pressure. Results show that for the TFC membrane in AL-FS, the values of the transport parameters *A*, *B* and *S* do not vary considerably between the two models and between the two membranes used in this investigation. The transport parameters *A*, *B* and *S* for the data associated with the experimental data set of Bai and Kruczek [16] are significantly lower than the ones obtained for Membranes 1 and 2 of this work. This is surprising because the water flux and the salt flux were nearly identical to those of Membranes 1 and 2 used in this work, as reported in Tables 3.1 and 3.2. The possible explanation is the correlation existing between the three parameters of the models. Indeed, suppose the value of the structural parameter *S* is lower for identical fluxes. In that case, this lower value of the mass transfer resistance of the porous layer will need to be compensated by smaller values of *A* and *B*. The same discrepancy applies to the AL-DS. One way to improve the estimation of the transport parameters is to have a larger number of experimental

runs at different draw solution concentrations to reduce the inherent run-to-run variability. In the current series of experiments, tests with only three different concentrations were performed.

The comparison of the values of the parameters for the two orientations (AL-DS and AL-FS) shows a good match for Membrane 2 but not for Membrane 1. Indeed, for Membrane 1, the parameters for the AL-DS are much higher. Again, it is possible that the correlation between the three parameters led to this discrepancy. In this case, a higher structural parameter *S* leads to higher permeance parameters *A* and *B* for the same water and salt fluxes. Given the variability in the data, it is paramount that additional experiments be performed at other draw solution concentrations. It should be noted that Membranes 1 and 2 had different cleaning protocols. The latter used the deionized water in the final cleaning runs, and as noted by Reyes et al. [15], it led to expected qualitative trends with the draw solution concentration.

The model developed in this investigation (Appendix B) has the advantage of a reduced number of assumptions. Still, on the other hand, it requires knowing more about the physical constitution of the membrane. The predicted water and salt permeances for the three sets of data are presented in Table 3.5 for the AL-FS orientation and in Table 3.6 for the AL-DS orientation. This model uses a unique, effective diffusivity of the porous layer independent of the membrane orientation. The equivalent parameter *S* remains constant for all experiments, which has for consequence to produce very consistent values of the water and salt permeances. For the AL-FS orientation, the three sets of data led to essentially the same permeances. For the AL-DS orientation, the values are very consistent for Membranes 1 and 2, but the values were twice as high for the data of Bai and Kruczek [16].

Table 3.3 Predicted intrinsic transport parameters for the three sets of experimental data using a TFC membrane in the AL-FS orientation with the models of Tiraferri et al. [3] and Martin et al. [9].

AL-FS	**Membrane 1**		**Membrane 2**		**Ref. [16]**	
	Tiraferri et al. (2013)	Martin et al. (2020)	Tiraferri et al. (2013)	Martin et al. (2020)	Tiraferri et al. (2013)	Martin et al. (2020)
A (L/m^2 h bar)	0.360	0.370	0.336	0.326	0.132	0.125
B (L/m^2 h)	0.229	0.229	0.226	0.219	0.082	0.077
S (um)	2865	2217	2914	2578	1394	1039

Table 3.4 Predicted intrinsic transport parameters for the three sets of experimental data using a TFC membrane in the AL-DS orientation with the models of Tiraferri et al. [3] and Martin et al. [9].

AL-DS	**Membrane 1**		**Membrane 2**		**Ref. [16]**	
	Tiraferri et al. (2013)	Martin et al. (2020)	Tiraferri et al. (2013)	Martin et al. (2020)	Tiraferri et al. (2013)	Martin et al. (2020)
A (L/m^2 h bar)	3.069	2.970	0.300	0.273	0.179	0.119
B (L/m^2 h)	2.175	2.110	0.471	0.428	0.267	0.214
S (um)	4262	4171	3720	3280	1104	616

Table 3.5 Predicted water and salt permeances for the three sets of experimental data using a TFC membrane in the AL-FS orientation with the model developed in this investigation.

AL-FS	**Membrane 1**	**Membrane 2**	**Ref. [16]**
A (L/m^2 h bar)	0.3185	0.3143	0.3018
B (L/m^2 h)	0.1237	0.1212	0.1186

Table 3.6. Predicted water and salt permeances for the three sets of experimental data using a TFC membrane in the AL-DS orientation with the model developed in this investigation.

AL-DS	**Membrane 1**	**Membrane 2**	**Ref. [16]**
A (L/m^2 h bar)	0.4518	0.4889	0.8474
B (L/m^2 h)	0.1627	0.1861	0.3341

3.4.1 Sensitivity Analysis

When using a model to describe the steady-state or dynamic behaviour of a process, it is essential to perform a sensitivity analysis of all model parameters to comprehend better the impact and the importance of each parameter on the model predictions. This analysis is vital because it allows identifying the most critical parameters that could be modified in the design of the membrane and the selection of the operating conditions. For instance, it was found that changing the mass transfer coefficient on the feed side of the membrane has a minor impact on the water and salt fluxes compared to other parameters, and it would be impossible to achieve better performance by only modifying the operating conditions on the feed side of the membrane. This

chapter reports on the sensitivity of the three transport parameters, namely *A*, *B* and *S*, which were determined to characterize the TFC membranes.

To perform this analysis, the nominal values of parameters *A*, *B* and *S* were determined from the non-linear regression analysis of the experimental data. Then, using these nominal values, one of these parameters was increased and decreased by 10 to 50% while the other two parameters remained unchanged, and the water flux (J_w) and salt flux (J_s) were calculated. Results of this sensitivity analysis are presented in Figure 3.2 for the model of Tiraferri et al. [3] and in Figure 3.3 for the model of Martin et al. [9]. Figures 3.2 and 3.3 present the results for the FO membrane orientation, but similar results were obtained for the PRO membrane orientation. Figures 3.2 and 3.3 also contain the experimental data, which allows seeing the fit of the data. As expected, Figure 3.2a shows that increasing the water permeance *A* leads to an increase in the water flux and vice versa. Based on Eq. (3-1), it would be tempting to deduce that the water flux is directly proportional to the water permeance parameter. However, this is not the case as Eq. (3-1) is implicit to the water flux and an increase of 50% in the water permeance parameter *A* leads to only a 10% increase of in the water flux. The reason for this interesting result is the impact of the water flux on the concentration polarization. Higher water permeance facilitates the permeation of water. At the same time, an increase in the water flux decreases the available salt concentration driving force (or osmotic pressure difference) across the active layer of the membrane. Figure 3.2d shows the impact of an increase of the water permeance *A* on the salt flux. One could logically think that increasing *A* should not affect the salt flux since *A* is not a parameter of Eq. (3-2). Results show that an increase in *A* leads to a decrease in the salt flux. This negative impact of *A* on the salt flux is due to the decrease in the salt driving force and the higher convective effect of water carrying some salt back to the draw solution.

Figures 3.2b and 3.2e present the effect of salt permeance *B* on the flux of water and salt, respectively. As suggested in Eq. (3-1), increasing permeance *B* does not affect the water flux. On the other hand, the flux of salt is directly impacted by salt permeance *B*. It is interesting to note that the salt flux was impacted more importantly by the water permeance *A* than by the salt permeance *B*. This result clearly shows the importance of the water flux on the flux of salt.

Figures 3.2c and 3.2f present the impact of the structural parameter *S* of the porous layer on the water and salt fluxes. An increase of *S* leads to a greater mass transfer resistance and a decrease

in both the water and salt fluxes. Akin to the effect of the water permeance parameter A, the structural parameter S has a much more significant impact on the salt flux than it has on the water flux.

Figure 3.3 presents an identical sensitivity analysis for the model proposed by Martin et al. [9]. When compared with the model of Tiraferri et al. [3], Martin et al. [9] have relaxed the assumption of the negligible mass transfer resistance in the two boundary layers of the membrane. The effect of A, B and S on J_w and J_s is very similar to the previous results, with only one notable difference for the salt flux. Indeed, the salt flux does not constantly increase, as was predicted by Tiraferri et al. [3]. Instead, the flux of salt reached a maximum at a salt concentration of about 4 M before starting to decrease slightly.

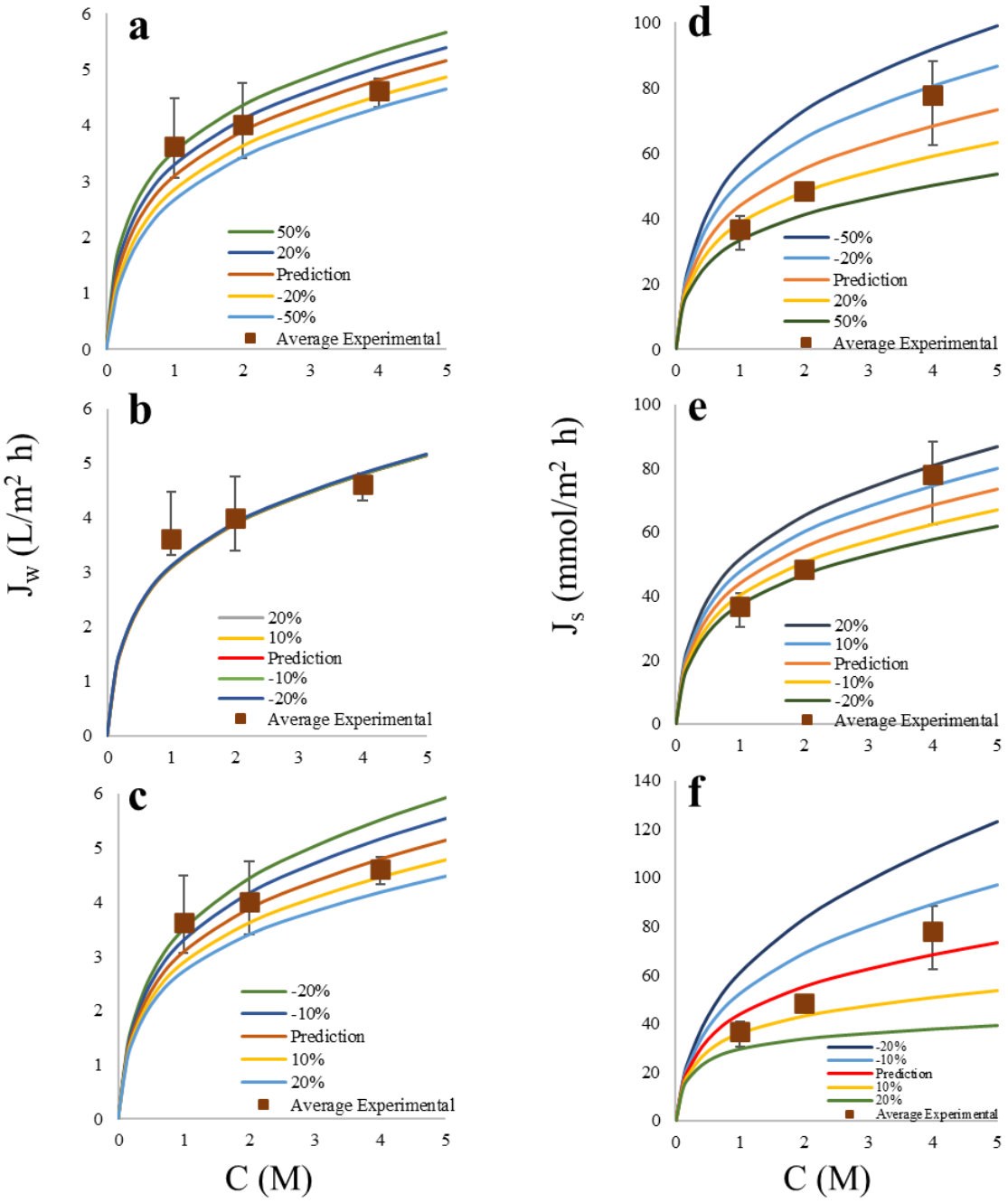

Figure 3.2 Effect of the variation of *A*, *B* and *S* on the water and salt fluxes using the model of Tiraferri et al. [3]: a) *A* on J_w, b) *B* on J_w, c) *S* on J_w, d) *A* on J_s, e) *B* on J_s, f) *S* on J_s.

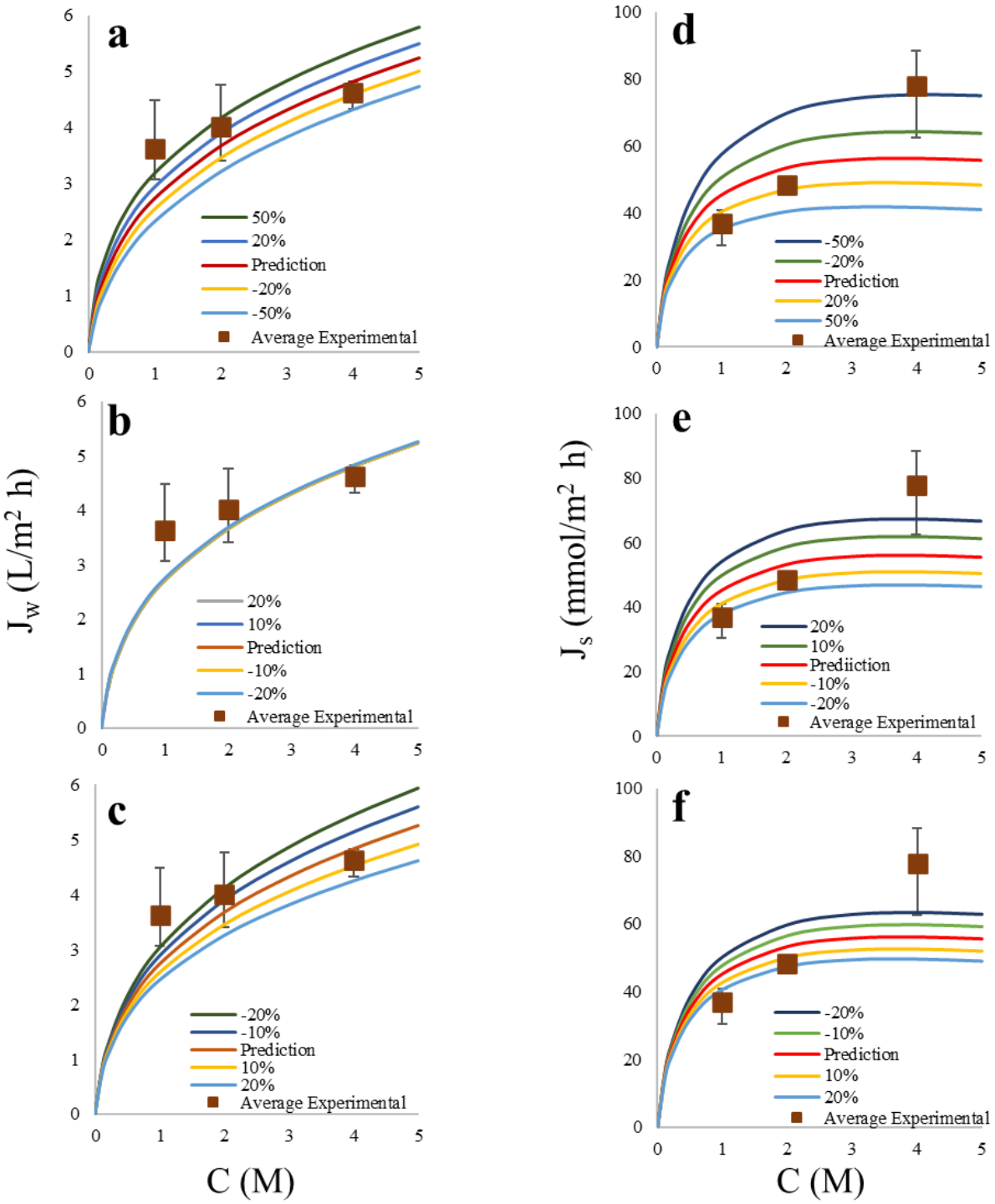

Figure 3.3 Effect of the variation of *A*, *B* and *S* on the water and salt fluxes using the model of Martin et al. [9]: a) *A* on J_w, b) *B* on J_w, c) *S* on J_w, d) *A* on J_s, e) *B* on J_s, f) *S* on J_s.

3.5 Conclusions

To characterize TFC membranes used for forward osmosis in an objective manner, three intrinsic transport parameters were calculated for each experiment performed in this work. These parameters are the water permeance *A*, the salt permeance *B* and the structural parameter of the porous support layer *S*. These parameters were estimated based on three sets of experimental data: two sets from this work and the data generated by Bai and Kruczek [16] using the same experimental FO system. All based on the first Fick's law of diffusion, three models were derived and used to identify the three transport parameters for each experiment using a TFC membrane. Two models were available in the literature, and one model was entirely derived in this work. Results showed that the parameters *A*, *B* and *S* were generally consistent from experiment to experiment, but some discrepancies were nonetheless observed. These discrepancies have attributed to the correlation existing between the parameters of the model. Finally, a sensitivity analysis was performed to assess the impact of the three transport parameters on the model prediction of the water and salt fluxes. This sensitivity analysis has revealed that any changes in the flux of water generated by a change in *A* and *S* impact the salt flux.

Nomenclature

A	Water permeance	L/m^2 h bar
B	Salt permeability	g/m^2 h
C	Concentration in the solution	mol/L, kg/m^3
C_1	In the AL-DS orientation, it represents the salt concentration in the bulk draw solution. In the AL-FS, it represents the salt concentration in the bulk feed solution.	mol/L
C_2	In the AL-DS orientation, it represents the salt concentration in the membrane surface at the active layer side towards the draw solution. In the AL-FS orientation, it represents the salt concentration in the membrane surface at the active layer side towards the feed solution.	mol/L
C_3	In the AL-DS and AL-FS orientations, it represents the salt concentration inside the membrane at the interface between the active layer and the porous support.	mol/L
C_4	In the AL-DS orientation, it represents the salt concentration in the membrane surface at the porous support layer side towards the feed solution. In the AL-FS orientation, it represents the salt concentration in the membrane surface at the porous support layer side towards the draw solution.	mol/L
C_5	In the AL-DS orientation, it represents the salt concentration in the bulk feed solution. In the AL-FS orientation, it represents the salt concentration in the bulk draw solution.	mol/L
D	Effective diffusion coefficient of the draw solute in the porous support, related to the D bulk diffusion coefficient	m^2/s
J_s	Salt flux	g/m^2 h, mmol/m2 h
J_w	Water flux	L/m^2 h
k_c	Mass transfer coefficient	m/s
L	Characteristic length	m
π	Osmotic pressure	bar
Re	Reynolds number	-
S	Structural parameter	m
Sc	Schmidt number	-
Sh	Sherwood number	-
T	Temperature	K

Subscripts

D	Draw solution
F	Feed solution
S	Salt
W	Water

Greek letters

ε	Porosity of the membrane	-
μ	Dynamic viscosity	kg/m s
ρ	Density	kg/m^3
τ	Tortuosity of the membrane	-
ν	Kinematic viscosity	m^2/s

Abbreviations

AL-DS	Active Layer facing the Draw Solution
AL-FS	Active Layer facing the Feed Solution
CP	Concentration Polarization
ECP	External Concentration Polarization
FO	It may refer to Forward Osmosis or to the membrane orientation in which the Active Layer is facing the Feed Solution
ICP	Internal Concentration Polarization
PRO	It may refer to Pressure Retarded Osmosis or to the membrane orientation in which the Active Layer is facing the Draw Solution
RO	Reverse Osmosis
TFC	Thin Film Composite Membrane

References

[1] B. Kim, G. Gwak, and S. Hong, "Review on methodology for determining forward osmosis (FO) membrane characteristics: Water permeability (A), solute permeability (B), and structural parameter (S)," *Desalination*, vol. 422, no. December 2015, pp. 5–16, 2017. shttps://doi.org/10.1016/j.desal.2017.08.006

[2] T. Sirinupong, W. Youravong, D. Tirawat, W. J. Lau, G. S. Lai, and A. F. Ismail, "Synthesis and characterization of thin film composite membranes made of PSF-TiO2/GO nanocomposite substrate for forward osmosis applications," *Arab. J. Chem.*, vol. 11, no. 7, pp. 1144–1153, 2018. https://doi.org/10.1016/j.arabjc.2017.05.006.

[3] A. Tiraferri, N. Y. Yip, A. P. Straub, S. Romero-Vargas Castrillon, and M. Elimelech, "A method for the simultaneous determination of transport and structural parameters of forward osmosis membranes," *J. Memb. Sci.*, vol. 444, pp. 523–538, 2013.iraferri, A., Yip, N. Y., Straub, A. P., Romero-Vargas Castrillon, S., & Elimelech, M. (2013). chttps://doi.org/10.1016/j.memsci.2013.05.023

[4] S. S. Manickam, J. Gelb, and J. R. McCutcheon, "Pore structure characterization of asymmetric membranes: Non-destructive characterization of porosity and tortuosity," *J. Memb. Sci.*, vol. 454, pp. 549–554, 2014.

[5] S. S. Manickam and J. R. McCutcheon, "Understanding mass transfer through asymmetric membranes during forward osmosis: A historical perspective and critical review on measuring structural parameter with semi-empirical models and characterization approaches," *Desalination*, vol. 421, pp. 110–126, 2017.

[6] B. D. Coday, D. M. Heil, P. Xu, and T. Y. Cath, "Effects of transmembrane hydraulic pressure on performance of forward osmosis membranes," *Environ. Sci. Technol.*, vol. 47, no. 5, pp. 2386–2393, 2013.Coday, B. D., Heil, D. M., Xu, P., & Cath, T. Y. (2013). ghttps://doi.org/10.1021/es304519p

[7] G. T. Gray, J. R. Mccutcheon, and M. Elimelech, "Internal concentration polarization in forward osmosis " role of membrane orientation," 2006. Desalination 197. Pages 1-8. https://doi.org/10.1016/j.desal.2006.02.003

[8] G. D. Mehta and S. Loeb, "Internal polarization in the porous substructure of a semipermeable membrane under pressure-retarded osmosis," *J. Memb. Sci.*, vol. 4, no. C, pp. 261–265, 1978. https://doi.org/10.1016/S0376-7388(00)83301-3

[9] J. T. Martin, G. Kolliopoulos, and V. G. Papangelakis, "An improved model for membrane characterization in forward osmosis," *J. Memb. Sci.*, vol. 598, no. November 2019, p. 117668, 2020.. https://doi.org/10.1016/j.memsci.2019.117668

[10] D. Bai, F. Asempour, and B. Kruczek, "Can the time-lag method be used for the characterization of liquid permeation membranes?," *Chem. Eng. Res. Des.*, vol. 162, no. 2, pp. 228–237, 2020. https://doi.org/10.1016/j.cherd.2020.08.012

[11] B. Djebedjian, H. Gad, I. Khaled and M. A. Rayan, "Optimization of Reverse Osmosis Desalination System," *12th Int. Water Technol. Conf.*, Alexandra, Egypt, pp. 1047–1067, 2008.

[12] J. R. Welty, C. E. Wicks, R. E. Wilson, G. L. Rorrer. Fundamentals of Momentum, Heat, and Mass Transfer. Wiley, *5th Edition*, 2008.

[13] N. Y. Yip , A. Tiraferri, W. A. Phillip, J. D. Schiffman, L. A. Hoover, Y. C. Kim, and M. Elimelech, "Thin-film composite pressure retarded osmosis membranes for sustainable power generation from salinity gradients," *Environ. Sci. Technol.*, vol. 45, no. 10, pp. 4360–4369, 2011. https://doi.org/10.1021/es104325z

[14] K. L. Lee, R. W. Baker, and H. K. Lonsdale, "Membranes for power generation by pressure-retarded osmosis," *J. Memb. Sci.*, vol. 8, no. 2, pp. 141–171, 1981. https://doi.org/10.1016/S0376-7388(00)82088-8

[15] S. Reyes, J. Thibault & B. Kruczek (2021). Improving accuracy of dynamic Forward Osmosis experiments. Paper to be submitted for publication.

[16] D. Bai, B. Kruczek, Effect of membrane orientation and concertation of draw solution on behaviors of commercial low-pressure RO membrane in novel dynamic forward osmosis tests, under review in Desalination.

Chapter 4. Conclusions and recommendations

This thesis was mainly focused on two aspects. First, improving the accuracy of FO experimental data was considered. Improved accuracy is paramount in order to perform the characterization of FO membranes by employing only FO data, thereby avoiding using a RO experimental system, thus reducing the number of steps for membrane characterization. Secondly, the improved FO experimental data was used to estimate three intrinsic membrane transport parameters, which characterize TFC membranes objectively.

In Chapter 2, a method for testing TFC membranes in a dynamic FO system was presented with the objective to improve the accuracy of the experimental results. The TFC membranes were tested employing the time-lag method previously developed (Bai et al., 2020), where eighteen membrane coupons were tested under identical experimental conditions as used in this investigation. The only difference between the experimental protocol of Bai et al. (2020) and this work is in the number of membrane coupons used. Bai et al. (2020) used eighteen different coupons, one for each experiment, whereas, in this work, a single membrane was used to generate the results of the similar eighteen different experiments. For the latter series of experiments, the membrane was thoroughly cleaned before performing the following experiment; two cleaning approaches were studied (Membrane 1 and Membrane 2). The objective was to eliminate the coupon-to-coupon variability.

Results showed that, when using deionized water in the final cleaning steps, the observed effect of the draw solution concentration on the different transport parameters followed the expected trends. On the other hand, when using distilled water for all cleaning steps, the expected trends were not fully reproduced. However, better adherence to the expected trends when using deionized water in the final cleaning steps did not translate to lower variation in the repeated experiments. The respective standard deviations observed in both cleaning protocols were comparable. The main objective remains to develop a cleaning approach as using washing water at high temperature to facilitate desorption of the draw solute from the membrane and the system, thus reducing the cleaning time.

In Chapter 3, the experimental data were fitted to mass transport model to determine three intrinsic transport parameters, namely the water permeance A, the salt permeance B and the

structural parameter of the porous layer *S*, in order to objectively characterize TFC membranes. Three mathematical models were used to fit the experimental data. Even though the intrinsic transport parameters were reasonably consistent, it is suggested to improve the accuracy of the transport parameters by increasing the number of experiments obtained at different concentrations of the draw solution. A sensitivity analysis has clearly shown the water permeance *A* and structural parameter *S* affects the flux of water in a lesser proportion as the flux of salt is affected. The water flux is subjected to a self-regulating effect whereby an increase in the flux of water increases the effect of concentration polarization, which tends to reduce the flux of water.

Further research should focus on improving the accuracy of the estimated values for *A*, *B* and *S*. This can be achieved by performing additional experimental tests under different conditions. The analysis performed in this thesis should be combined with the fabrication of FO membranes in our laboratory, such that a synergetic approach is used. It is also envisaged to add an option in the model developed in this investigation to allow performing a series of numerical experiments from known values of the water and slat permeances, thereby enhancing the sensitivity analysis.

Appendix A

Steady-state derivation to calculate the fluxes of water and salt across a thin-film composite membrane [1], [2].

Introduction

A schematic representation of a typical salt concentration profile across a thin-film composite (TFC) membrane operating in pressure-retarded osmosis (PRO) mode is shown in Figure A.1. PRO mode prevails when the active layer faces the draw solution. When the active layer is adjacent to the feed solution, the mode of operation is said to be forward osmosis (FO).

The TFC membrane described in Figure A.1 consists of two layers. The left layer is known as the active layer, which is a thin semipermeable layer designed to significantly limit the permeation of salt while remaining permeable to water. The right layer is the support layer that is porous and thicker than the active layer. In Figure A.1, for the membrane system operating in PRO mode, the salt solution or draw solution flows on left-hand side of the active layer and the feed solution flows on the right-hand side of the two-layer membrane. As a result, there exists a boundary layer from both sides of the membrane system. Because of the difference of concentration for both water and salt on the two sides of the two-layer membrane, water flows from the feed solution to the draw solution whereas some salt flows in the opposite direction.

In Figure A.1, C_1 represents the concentration of salt in the draw solution. In this work, the draw solution was a NaCl solution. C_2 represents the concentration of salt in the boundary layer of the draw solution at the surface of the membrane. C_3 represents the concentration of salt in the porous layer at the interface between the active layer and the porous support layer. C_4 corresponds to the concentration of salt in the feed solution. It is assumed that the boundary layer on the feed solution is negligible. This is a valid assumption in the present study as deionized distilled water was used as the feed solution for all experiments. In our experiments, concentrations of the draw and feed solutions were monitored whereas concentrations C_2 and C_3 cannot be measured experimentally. These latter concentrations are required to estimate the permeability or the permeance of the thin film semipermeable active layer. To access these two concentrations, it is necessary to consider

the mass transfer resistances for the boundary layer and the porous layer. These resistances lead to a decrease in the steady-state water flux due to the decrease of the concentration gradient or in the difference in osmotic pressure across the active layer. This decrease in the effective osmotic pressure across the active layer are therefore due to the external concentration polarization (ECP) and internal concentration polarization (ICP).

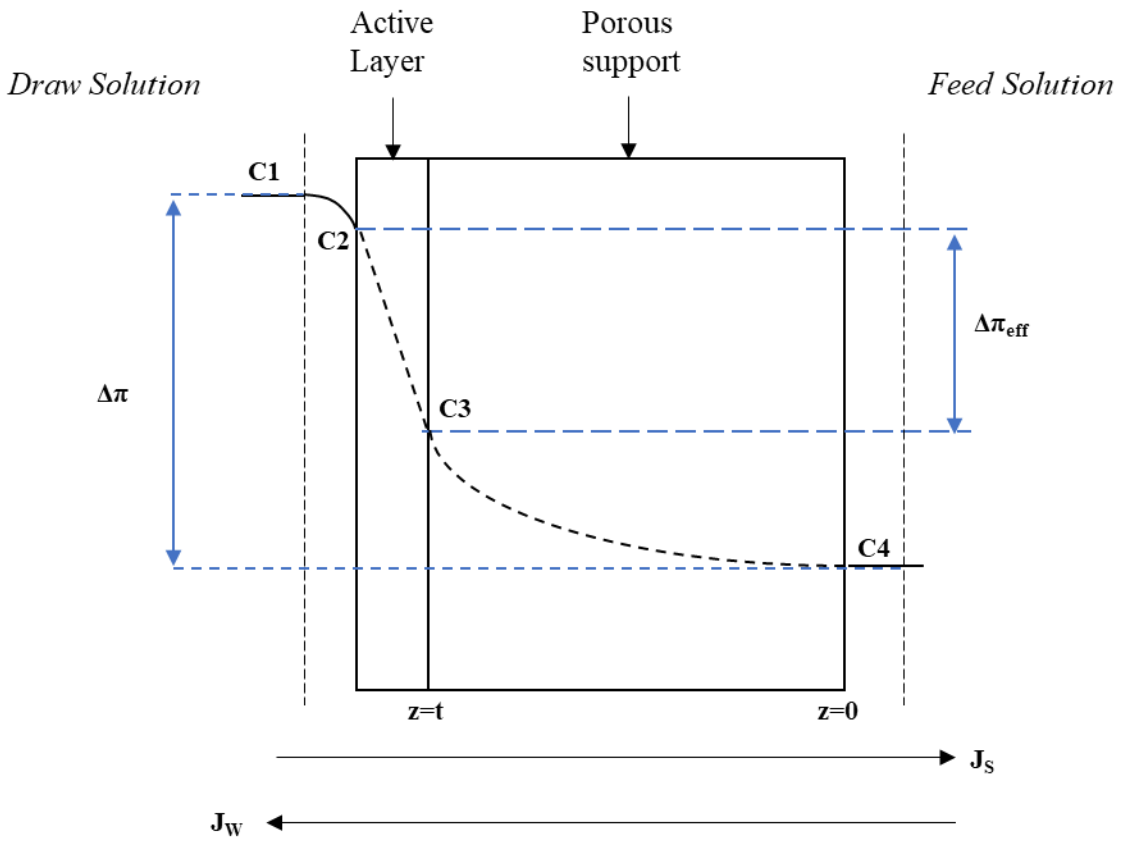

Figure A.1 Schematic diagram of salt concentration profile under steady state in a TFC membrane in PRO mode.

Earlier studies to derive the water flux equation in the PRO mode did not take the ECP into account even though it was deemed important [11],[12]. The complete derivation of the equation used to describe the water flux considering both the ICP and ECP is presented next. At the same time, an equation to estimate the salt flux is also derived in this appendix.

The system of Figure A.1 is a one-dimensional system, and the flow of water and salt can be described mathematically using the Fick's first law diffusion equation (Eq. A-1). This equation

applies for the boundary layer adjacent to the active layer and the two layers of the membrane, where diffusion and convection coexist. The diffusion coefficients are different for each of the three sections of the membrane whereas, under steady state, the water and salt fluxes are constant throughout all sections of the membrane system.

$$J_w = -cD_w \frac{dx_w}{dz} + x_w\left(J_w + J_s\right) \tag{A-1a}$$

$$J_s = -cD_s \frac{dx_s}{dz} + x_s\left(J_w + J_s\right) \tag{A-1b}$$

J_w is the water flux (kg/m^2 s), J_s is the salt flux (kg/m^2 h), c is the total concentration (kg/m^3), D is the diffusion coefficient (m^2/s), and x is mass fraction (kg/kg). Subscripts w and s designate water or salt, respectively. The units of these equations are slightly different from the one in the main body of this chapter but it is an easy change of units to go from one equation to the other.

Water and salt fluxes across the active layer.

The steady state water flux (kg/m^2 s) across the active layer is often defined as a function of the net pressure difference across the active layer as described by Eq. (A-2) where both the osmotic pressure and hydraulic pressure are considered. The concentration in the Fick's equation was converted into osmotic pressure to be in the same units as the hydraulic pressure.

$$J_w = A(\Delta\pi_m - \Delta P) = A\left[\left(\pi_2 - \pi_3\right) - \Delta P\right] \tag{A-2}$$

where A is the water permeance coefficient (kg/m^2 s bar), $\Delta\pi_m$ is the effective osmotic pressure across the active layer (bar), and ΔP is the applied hydraulic pressure difference across the membrane (bar). ΔP is positive when the static pressure on the draw side of the membrane is greater than for the feed side.

Salt permeates across the membrane in the opposite direction of the water flux, from the draw solution to the feed solution. For this reason, a negative sign has been added for the salt flux (kg/m^{2}s) represented using Eq. (A-3).

$$J_s = -B(C_2 - C_3) = -cB(x_2 - x_3) \tag{A-3}$$

where B is the salt permeance coefficient of the membrane (m/s), C_2 is the salt concentration (kg/m^3) in the draw solution at the membrane interface and C_3 is the salt concentration in the solution in the porous layer at the interface between the active and porous layers. Ideally, B should be very small or even negligible; however, no membranes are perfect and a salt flux will exist. Eq. (A-3) in terms of concentration is most often used in the literature, but it could well be defined in terms of mass fractions x_2 and x_3 as seen in the last term of Eq. (A-3) with the assumption that the total concentration or total density is constant.

It is important to mention that Eqs. (A-2) and (A-3) were defined with the assumption that convective term of the Fick equation is negligible. The permeance values of A and B will therefore incorporate this assumption.

Mass transfer in the porous support layer

In the porous layer, the same steady-state fluxes of water and salt as in the other sections of the membrane prevail in opposing direction. Because the flux of water is larger than the flux of salt, some salt is entrained back by the water flow, thereby creating an accumulation at the interface with the active layer. This is an addition to the semi-impermeability property of the membrane that inhibits the passage of salt across the thin active layer. This higher salt concentration at the interface of the active layer dictates the driving force to accommodate a constant salt flux via diffusion. In addition, the higher salt concentration at the interface reduces the effective osmotic pressure difference across the active layer, referred to as concentration polarization. The porous membrane layer acts as an unstirred tortuous boundary layer and has a significant impact on the magnitude of the internal concentration polarization (ICP).

As subjected to the Fick's first law of diffusion, the salt flux across the porous support is the sum of the diffusive component, driven by the salt concentration gradient, and the opposing convective component arising from the bulk flow of water through the membrane, as expressed in Eq. (A-4). In Eq. (A-4), it is assumed that the salt flux is much smaller than the water flux such that its contribution has been neglected in the convective term of the Fick's equation.

$$J_s = cD_s \frac{dx_s}{dz} - x_s J_w \qquad \text{(A-4)}$$

Under steady state, the salt flux across the active and support layers are equal. Eqs. (A-3) and (A-4) are therefore combined to give Eq. (A-5).

$$J_s = \mathrm{cD}_s \frac{dx_s}{dz} - x_s J_w = B(C_2 - C_3) \tag{A-5}$$

The diffusion coefficient in Eq. (A-5) is the effective salt diffusion coefficient that takes into account the diffusion of salt in water corrected by the void fraction of the porous membrane and the membrane tortuosity as defined in Eq. (A-6).

$$\mathrm{D}_s = \frac{D\varepsilon}{\tau} \tag{A-6}$$

Integrating Eq. (A-5) across the support layer from the porous layer-feed solution interface at z=0, where the salt concentration is equal to C_4 (i.e. a mass fraction x_4) to the porous layer-active layer interface, z=t_3 where the salt concentration is C_3 (i.e. a mass fraction x_3) yields:

$$\int_{x_4}^{x_3} \frac{dx_s}{B(C_2 - C_3) + x_s J_w} = \int_0^{t_3} \frac{dz}{\mathrm{cD}_s} \tag{A-7}$$

Mathematical reminder:

$$\int_{x_4}^{x_3} \frac{dx}{a + bx} = \frac{1}{b} \ln[a + bx] \Big|_{x_4}^{x_3} \tag{A-8}$$

For our equation, we therefore get

$$\frac{1}{J_w} \ln\left[\frac{B(C_2 - C_3) + x_3 J_w}{B(C_2 - C_3) + x_4 J_w}\right] = \frac{t_3}{\mathrm{cD}_s} \tag{A-9}$$

A geometrical parameter S for the porous layer is now defined using Eq. (A-6).

$$\frac{t_3}{cD_s} = \frac{t_3 \tau}{cD\varepsilon} = \frac{S}{cD} \tag{A-10}$$

Eq. (A-9) now becomes:

$$\ln\left[\frac{B(C_2 - C_3) + x_3 J_w}{B(C_2 - C_3) + x_4 J_w}\right] = \frac{J_w S}{\mathrm{cD}} \tag{A-11}$$

Taking the exponential for the right-hand and left-hand sides:

$$\frac{B(C_2 - C_3) + x_3 J_w}{B(C_2 - C_3) + x_4 J_w} = \mathrm{e}^{\frac{J_w S}{\mathrm{cD}}} \tag{A-12}$$

$$B(C_2 - C_3) + x_3 J_w = \left(B(C_2 - C_3) + x_4 J_w\right)\mathrm{e}^{\frac{J_w S}{\mathrm{cD}}} \tag{A-13}$$

$$x_3 J_w = x_4 J_w e^{\frac{J_w S}{cD}} + B(C_2 - C_3)\left(e^{\frac{J_w S}{cD}} - 1\right) \tag{A-14}$$

$$x_3 = x_4 e^{\frac{J_w S}{cD}} + \frac{B}{J_w}(C_2 - C_3)\left(e^{\frac{J_w S}{cD}} - 1\right) \tag{A-15}$$

This equation could also be written to include the salt flux (Eq. (A-16)) to estimate the mass fraction x_3 when the water and salt fluxes, and the geometrical parameter S.

$$x_3 = x_4 e^{\frac{J_w S}{cD}} + \frac{J_s}{J_w}\left(e^{\frac{J_w S}{cD}} - 1\right) \tag{A-16}$$

If the assumption of a negligible ECP is made, Eqs. (A-2) and (A-15) provide the information required to estimate the permeance parameters A and B as well as the geometrical parameter S. With this assumption, the mass fraction in the draw solution x_1 is equal to the mass fraction x_2 at the interface of the active layer.

Mass transfer in the draw solution boundary layer

If it is desired to include the external concentration polarization (ECP), the previous analysis can be adapted for the migration of water and salt in the boundary layer in the draw solution starting with Eq. (A-4). Indeed, under steady state, the salt flux in the boundary layer (Eq. (A-4)) is equal to the salt flux across the active layer (Eq. (A-3)). Integrating the resulting equation across the ECP boundary layer from the active layer $z = t_2$, where the salt concentration is C_2 to the bulk draw solution, z = t_1 where the salt concentration is C_1. The boundary layer thickness $\delta = t_2 - t_1$.

$$J_s = \mathrm{cD}_s \frac{dx_s}{dz} - x_s J_w = B(C_2 - C_3) \tag{A-17}$$

Let us integrate Eq. (A-17) from $z = t_2$ with mass fraction x_2 to $z = t_1$ with mass fraction x_1 gives:

$$\int_{x_2}^{x_1} \frac{dx_s}{B(C_2 - C_3) + x_s J_w} = \int_{t_2}^{t_1} \frac{dz}{\mathrm{cD}_s} \tag{A-18}$$

$$\frac{1}{J_w} \ln\left[\frac{B(C_2 - C_3) + x_1 J_w}{B(C_2 - C_3) + x_2 J_w}\right] = \frac{t_2 - t_1}{\mathrm{cD}_s} \tag{A-19}$$

$$\ln\left[\frac{B(C_2 - C_3) + x_1 J_w}{B(C_2 - C_3) + x_2 J_w}\right] = \frac{\delta J_w}{\mathrm{cD}_s} \tag{A-20}$$

Taking the exponential for the right-hand and left-hand sides with D_s = D since there is no tortuosity and void.

$$\frac{B(C_2 - C_3) + x_1 J_w}{B(C_2 - C_3) + x_2 J_w} = \mathrm{e}^{\frac{\delta J_w}{\mathrm{cD}}} \tag{A-21}$$

It is possible to express the diffusion across the boundary layer in terms of the mass transfer coefficient:

$$k = \frac{D}{\delta} \tag{A-22}$$

$$\frac{B(C_2 - C_3) + x_1 J_w}{B(C_2 - C_3) + x_2 J_w} = e^{\frac{J_w}{ck}} \tag{A-23}$$

$$x_2 J_w = B(C_2 - C_3) e^{-\frac{J_w}{ck}} + x_1 J_w e^{-\frac{J_w}{ck}} - B(C_2 - C_3) \tag{A-24}$$

$$x_2 J_w = B(C_2 - C_3)\left(e^{-\frac{J_w}{ck}} - 1\right) + x_1 J_w e^{-\frac{J_w}{ck}} \tag{A-25}$$

$$x_2 = \frac{B}{J_w}(C_2 - C_3)\left(e^{-\frac{J_w}{ck}} - 1\right) + x_1 e^{-\frac{J_w}{ck}} \tag{A-26}$$

Putting the equations together

C_2 and C_3 or x_2 and x_3 are not measured experimentally and the previous equations can be rearranged to obtain equations that will only depend on the two bulk concentrations. We first subtract Eq. (A-26) from Eq. (A-15).

$$x_3 - x_2 = \left[x_4 e^{\frac{J_w S}{cD}} + \frac{cB}{J_w}(x_2 - x_3)\left(e^{\frac{J_w S}{cD}} - 1\right)\right] - \left[\frac{cB}{J_w}(x_2 - x_3)\left(e^{-\frac{J_w}{ck}} - 1\right) + x_1 e^{-\frac{J_w}{ck}}\right] \tag{A-27}$$

$$x_2 - x_3 = \left[x_1 e^{-\frac{J_w}{ck}} - x_4 e^{\frac{J_w S}{cD}}\right] + \left[\frac{cB}{J_w}(x_2 - x_3)\left(e^{-\frac{J_w}{ck}} - 1\right) - \frac{cB}{J_w}(x_2 - x_3)\left(e^{\frac{J_w S}{cD}} - 1\right)\right] \tag{A-28}$$

$$x_2 - x_3 = \left[x_1 e^{-\frac{J_w}{ck}} - x_4 e^{\frac{J_w S}{cD}}\right] + \frac{cB}{J_w}(x_2 - x_3)\left[\left(e^{-\frac{J_w}{ck}} - 1\right) - \left(e^{\frac{J_w S}{cD}} - 1\right)\right] \tag{A-29}$$

$$(x_2 - x_3)\left[1 - \frac{cB}{J_w}\left[e^{-\frac{J_w}{ck}} - e^{\frac{J_w S}{cD}}\right]\right] = \left[x_1 e^{-\frac{J_w}{ck}} - x_4 e^{\frac{J_w S}{cD}}\right] \tag{A-30}$$

$$(x_2 - x_3) = \frac{x_1 e^{-\frac{J_w}{ck}} - x_4 e^{\frac{J_w S}{cD}}}{1 + \frac{cB}{J_w}\left[e^{\frac{J_w S}{cD}} - e^{-\frac{J_w}{ck}}\right]} \tag{A-31}$$

Assuming that the osmotic pressure is directly proportional to the salt concentration, the Van't Hoff equation can be used to convert the salt concentrations or mass fractions to osmotic pressures. All concentrations in Eq. (A-31) can then be converted to osmotic pressure and use Eq. (A-2) to express the effective concentration difference across the membrane in term of the water flux, thereby eliminating the two unknowns.

The effective osmotic pressure $\Delta\pi_m$ is proportional to the difference in concentration:

$$\Delta C_m = c_2 - c_3 \tag{A-32}$$

$$\Delta\pi_m = \pi_2 - \pi_3 \tag{A-33}$$

$$J_w = A(\pi_2 - \pi_3) - A\Delta P \tag{A-34}$$

$$c\left(x_2 - x_3\right) = \frac{cx_1 e^{-\frac{J_w}{ck}} - cx_4 e^{\frac{J_w S}{cD}}}{1 + \frac{cB}{J_w}\left[e^{\frac{J_w S}{cD}} - e^{-\frac{J_w}{ck}}\right]} \tag{A-35}$$

$$\left(\pi_2 - \pi_3\right) = \frac{\pi_1 e^{-\frac{J_w}{ck}} - \pi_4 e^{\frac{J_w S}{cD}}}{1 + \frac{cB}{J_w}\left[e^{\frac{J_w S}{cD}} - e^{-\frac{J_w}{ck}}\right]} \tag{A-36}$$

$$A\left(\pi_2 - \pi_3\right) = \mathrm{A}\left[\frac{\pi_1 e^{-\frac{J_w}{ck}} - \pi_4 e^{\frac{J_w S}{cD}}}{1 + \frac{cB}{J_w}\left[e^{\frac{J_w S}{cD}} - e^{-\frac{J_w}{ck}}\right]}\right] \tag{A-37}$$

$$J_w = A\left[\frac{\pi_1 e^{-\frac{J_w}{ck}} - \pi_4 e^{\frac{J_w S}{cD}}}{1 + \frac{cB}{J_w}\left[e^{\frac{J_w S}{cD}} - e^{-\frac{J_w}{ck}}\right]}\right] - A\Delta P \tag{A-38}$$

Similarly, for the salt flux, we have

$$J_s = \mathrm{cB}\left[\frac{x_1 e^{-\frac{J_w}{ck}} - x_4 e^{\frac{J_w S}{cD}}}{1 + \frac{cB}{J_w}\left[e^{\frac{J_w S}{cD}} - e^{-\frac{J_w}{ck}}\right]}\right] \tag{A-39}$$

These are the two final equations that were used to identify parameters A, B and S for each experimental run performed in this work.

Appendix B

Steady-state derivation of NaCl concentration profile across a membrane in PRO mode

The schematic diagram of a thin-film composite (TFC) membrane in PRO mode with the two adjacent boundary layers is presented in Figure B.1. The PRO mode corresponds to the membrane orientation for which the active layer is facing the draw solution. C_1 represents the concentration of salt in the draw solution; C_1 is a known variable. C_2 represents the concentration of salt in the solution at the interface between the boundary layer of the draw solution and the active layer; this concentration cannot be measured experimentally and must be calculated. C_3 is the concentration of salt in the solution in the porous layer at the interface between the porous support and the active layer; akin to concentration C_2, concentration C_3 cannot be measured experimentally and must be calculated. C_4 is the concentration of salt at the interface of the porous layer and the boundary layer on the feed side. Technically, concentration C_4 cannot be measured experimentally, but it is mostly assumed to be equal to the salt concentration of the feed solution. In our series of experiment, designed to study and characterize the TFC membrane, it was assumed that the feed solution was comprised of pure deionized water, such that the concentration of salt in the feed solution (C_5) is zero. The assumption that C_4 is nearly equal to C_5 is justified because the mass transfer resistance in the boundary layer adjacent to the porous layer is very small compared to the mass transfer resistances of the active and porous layers.

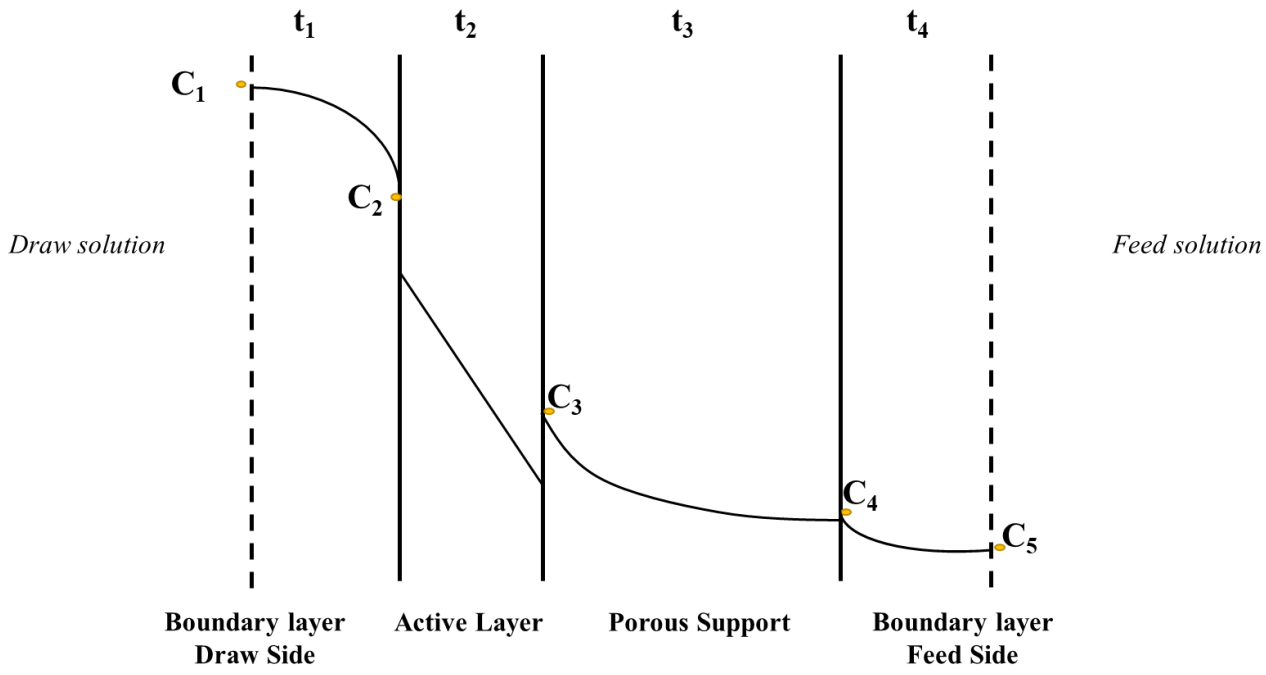

Figure B.1 Schematic diagram of a TFC membrane in PRO mode (active layer facing the draw solution) showing the active and porous layers along with the two adjacent boundary layers.

Because of the difference in the salt concentration on both sides of the membrane, there is a driving force giving rise to a salt flux going from the draw to the feed solution. Conversely, the higher concentration of water on the feed side creates a driving force for the migration of water from the feed side to the draw side. This difference in water concentration is most commonly expressed as a difference in osmotic pressure. The flux of salt and water are in opposite direction and the flux of water is much greater than the flux of salt because the active layer is much more permeable to water than it is for salt. For an ideal semi-permeable membrane, the flux of salt would be negligible. The main resistance to mass transfer is due to the active layer. To study and characterize membranes, it is therefore necessary to determine the permeability of the active layer for water and salt. To determine the permeability of water and salt for the active layer, it is required to determine the concentration in the solution on both sides of this active layer. In a typical experiment, the flux of salt, the flux of water, concentration C_1 and concentration C_5 are available. With these four known variables and some applicable mass transfer equations, it is possible to determine concentrations C_2 and C_3, from which the permeability of the active layer can be determined. The derivation was divided into two sets of equations: (1) the derivation of the film

diffusion in the boundary layer on the draw side and in the porous support layer, and (2) the derivation of the permeation flux across the active layer.

For all the layers in Figure B1, the first Fick equation of diffusion applies, where diffusion and convection coexist. On the other hand, for the active layer, it will be assumed that the permeability parameter will embed both diffusion and convection.

Starting with the first Fick's law of diffusion with subscripts A and B representing salt and water, respectively.

$$N_A = -cD_{AB}\frac{dX_A}{dz} + X_A(N_A + N_B) \qquad (B-1)$$

$$cD_{AB}\frac{dX_A}{dz} = X_A(N_A + N_B) - N_A \qquad (B-2)$$

$$cD_{AB}\frac{dX_A}{X_A(N_A + N_B) - N_A} = dz \qquad (B-3)$$

$$\int_{z_1}^{z_2} dz = cD_{AB}\int_{XA_1}^{XA_2}\frac{dX_A}{X_A(N_A + N_B) - N_A} \qquad (B-4)$$

$$(z_2 - z_1) = cD_{AB}\frac{1}{(N_A + N_B)}ln\left(\frac{X_{A2}(N_A + N_B) - N_A}{X_{A1}(N_A + N_B) - N_A}\right) \qquad (B-5)$$

$$\frac{(N_A + N_B)(z_2 - z_1)}{cD_{AB}} = ln\left(\frac{X_{A2}(N_A + N_B) - N_A}{X_{A1}(N_A + N_B) - N_A}\right) \qquad (B-6)$$

$$\frac{X_{A2}(N_A + N_B) - N_A}{X_{A1}(N_A + N_B) - N_A} = exp\left(\frac{(N_A + N_B)(z_2 - z_1)}{cD_{AB}}\right) \qquad (B-7)$$

$$X_{A2}(N_A + N_B) - N_A = (X_{A1}(N_A + N_B) - N_A)\left[exp\left(\frac{(N_A + N_B)(z_2 - z_1)}{cD_{AB}}\right)\right] \qquad (B-8)$$

$$X_{A2} = \frac{N_A}{(N_A + N_B)} + \left(X_{A1} - \frac{N_A}{(N_A + N_B)}\right)\left[exp\left(\frac{(N_A + N_B)(z_2 - z_1)}{cD_{AB}}\right)\right] \qquad (B-9)$$

$$X_{A2} = \frac{N_A}{(N_A + N_B)} + \left(X_{A1} - \frac{N_A}{(N_A + N_B)}\right)exp\left(\frac{(N_A + N_B)(z_2 - z_1)}{cD_{AB}}\right) \qquad (B-10)$$

More generally for any value of *z*, this equation can be written as follows and allows to calculate the concentration profile across a specific layer.

$$\boldsymbol{X_A = \frac{N_A}{(N_A + N_B)} + \left(X_{A1} - \frac{N_A}{(N_A + N_B)}\right) exp\left(\frac{(N_A + N_B)(z - z_1)}{cD_{AB}}\right)} \quad (\boldsymbol{B - 11})$$

A similar equation can also be written for water (B).

Mass transfer across the active layer (Layer 2)

Starting with the first Fick´s law of diffusion.

$$N_A = -cD_{AB}\frac{dX_A}{dz} + X_A(N_A + N_B) \quad (B - 12)$$

Assuming that the flux of water and salt are independent of each other, this equation can be reduced to the following equation. In addition, the concentration in the Fick equation is the concentration inside the active layer, which can be expressed in terms of the concentration in the solution in contact with the active layer using the appropriate constant solubility coefficient S_A.

$$N_A = -D_{AB}\frac{dC_A^{i,In}}{dz} = -D_{AB}\frac{d\left(S_A C_A^{i,Out}\right)}{dz} \quad (B - 13)$$

$$N_A = -D_{AB}S_A\frac{dC_A^{i,Out}}{dz} = -P_A\frac{dC_A^{i,Out}}{dz} \quad (B - 14)$$

The product of the diffusivity and solubility is equal to the permeability P_A of the membrane.

$$dC_A^{i,Out} = -\frac{N_A}{P_A}dz \quad (B - 15)$$

$$\int_{C_{A2}}^{C_{A3}} dC_A^{i,Out} = -\frac{N_A}{P_A}\int_{z_2}^{z_3} dz \quad (B - 16)$$

$$C_{A3}^{i,Out} - C_{A2}^{i,Out} = -\frac{N_A}{P_A}(z_3 - z_2) \quad (B - 17)$$

$$\boldsymbol{C_{A3}^{i,Out} = C_{A2}^{i,Out} - \frac{N_A}{P_A}(z_3 - z_2)} \quad (\boldsymbol{B - 18})$$

Eq. (B-18) allows calculating the permeability when the concentration on both side of the membrane has been determined and the flux and thickness are known. This equation applies equally well for water and salt.

References

[1] N. Y. Yip , A. Tiraferri, W. A. Phillip, J. D. Schiffman, L. A. Hoover, Y. C. Kim, and M. Elimelech, “Thin-film composite pressure retarded osmosis membranes for sustainable power generation from salinity gradients,” *Environ. Sci. Technol.*, vol. 45, no. 10, pp. 4360–4369, 2011. https://doi.org/10.1021/es104325z

[2] K. L. Lee, R. W. Baker, and H. K. Lonsdale, “Membranes for power generation by pressure retarded osmosis,” *J. Memb. Sci.*, vol. 8, no. 2, pp. 141–171, 1981. https://doi.org/10.1016/S0376-7388(00)82088-8